Research Article | Vol. 11, No. 8 / 1 August 2020 / Biomedical Optics Express 4602
Biomedical Optics EXPRESS

Dynamic microcirculation PIPE model for functional neuroimaging, non-neuroimaging, and coherent hemodynamics spectroscopy: blood volume and flow velocity variations, and vascular autoregulation

M. Xu,[1,2,*] Yang Zheng,[1] Xinlin Chen,[1] Ying Li,[1] Weihao Lin,[1] and Bixin Zeng[1]

[1] *Institute of Lasers and Biomedical Photonics, Biomedical Engineering College, Wenzhou Medical University, Wenzhou, Zhejiang, 325035, China*
[2] *Dept. of Physics and Astronomy, Hunter College and the Graduate Center, The City University of New York, 695 Park Ave, New York, NY 10065, USA*
[*] *minxu@hunter.cuny.edu*

Abstract: We present a dynamic microcirculation PIPE model for functional neuroimaging, non-neuroimaging, and coherent hemodynamics spectroscopy. The temporal evolution of the concentration and oxygen saturation of hemoglobin in tissue, comprised of the contributions from the arterioles, capillaries, and venules of microvasculature, is determined by time-resolved hemodynamic and metabolic variations in blood volume, flow velocity, and oxygen consumption with a fluid mechanics treatment. Key parameters regarding microcirculation can be assessed, including the effective blood transit times through the capillaries and the venules, and the rate constant of oxygen release from hemoglobin to tissue. The vascular autoregulation can further be quantified from the relationship between the resolved blood volume and flow velocity variations. The PIPE model shows excellent agreement with the experimental cerebral and cutaneous coherent hemodynamics spectroscopy (CHS) and fMRI-BOLD data. It further identifies the impaired cerebral autoregulation distinctively in hemodialysis patients compared to healthy subjects measured by CHS. This new dynamic microcirculation PIPE model provides a valuable tool for brain and other functional studies with hemodynamic-based techniques. It is instrumental in recovering physiological parameters from analyzing and interpreting the signals measured by hemodynamic-based neuroimaging and non-neuroimaging techniques such as functional near-infrared spectroscopy (fNIRS) and functional magnetic resonance imaging (fMRI) in response to brain activation, physiological challenges, or physical maneuvers.

1. Introduction

The study of cerebral hemodynamic oscillations, both spontaneous and induced, has led to a series of important results that opened new opportunities for the investigation of brain function, physiology, and pathological conditions. The spontaneous low-frequency oscillations (LFOs) ($\lesssim$0.1 Hz) and induced oscillations by maneuvers such as paced breathing [1], repeated head-up tilting [2], squat-stand [3], and cyclic thigh cuff inflation-deflation [4] reflect a combination of systemic cardiovascular dynamics and local metabolic and flow regulation effects. Spontaneous low-frequency oscillation studies have been used to assess, for example, resting-state functional connectivity using functional magnetic resonance imaging (fMRI) [5] and functional near-infrared spectroscopy (fNIRS) [6], rest versus functional activation [7], different sleep stages [8], and cerebral autoregulation [9]. As the induced cerebral hemodynamic oscillations feature a significantly stronger coherence and reliability than spontaneous LFOs, induced oscillation

#396817 https://doi.org/10.1364/BOE.396817
Journal © 2020 Received 5 May 2020; revised 11 Jun 2020; accepted 18 Jun 2020; published 24 Jul 2020

Biomedical Optics EXPRESS

studies have recently been actively pursued to assess and quantify physiological parameters related to the cerebral microcirculation [10,11].

As hemodynamics is complex, a successful model identifies a set of key parameters and reproduces the salient features of observations with a necessarily simplified description of the dynamic features of the vasculature, blood flow, and oxygen delivery to tissue. Well-known examples include the dynamic balloon model [12] and a Windkessel model [13], playing pivotal roles in interpreting the fMRI BOLD signal and fNIRS optical signals. Recently, Fantini [10] presented a dynamic model to relate tissue concentration and saturation of hemoglobin to hemodynamic and metabolic processes involving different vascular compartments. The three key parameters are blood volume oscillation phasor, flow velocity phasor, and the metabolic rate of oxygen. The Fantini model itself does not make specific constraints regarding the phase relations between the oxy- and deoxy-hemoglobin volume oscillation phasors and the oxy- and deoxy-hemoglobin flow oscillation phasors. Simplifications were, however, typically introduced when applied to the analysis of experimental data that the oxy- and deoxy-hemoglobin volume oscillation phasors (OV, DV) are in phase and the oxy- and deoxy-hemoglobin flow velocity oscillation phasors (OF, DF) are out-of-phase. The combination of contributions from arterial, capillary, and venous compartments then determines the microcirculation hemodynamics. This Fantini model has been successfully applied to neuroimaging, in particular, monitoring the cerebral microcirculation variations between hemodialysis patients and healthy subjects [14], cerebral autoregulation [15], and cerebral blood flow [16].

The phase relation between the oxy- and deoxy-hemoglobin volume oscillation phasors (OV, DV) and the oxy- and deoxy-hemoglobin flow velocity oscillation phasors (OF, DF) are in reality determined by the oxygen consumption occurring over the whole trajectory along which the red blood cells (RBC) move from the arterioles, through capillaries and then to the venous compartment while exchanging oxygen with the surrounding tissue. The true phase differences between both volume oscillation phasors and flow velocity phasors deviate from the above simplification made in the application of the Fantini model in general.

In this article, we present a dynamic microcirculation PIPE model for functional neuroimaging, non-neuroimaging, and coherent hemodynamics spectroscopy. The arterioles, capillaries, and venules are treated as a complete network (*compliant* pipe) through which the total hemoglobin is conserved. Without making assumptions on the details of the architecture and morphology of the microvascular bed, the temporal evolution of the concentration and oxygen saturation of hemoglobin in tissue in the PIPE model is determined by the superposition of time-resolved hemodynamic and metabolic variations in blood volume, flow velocity, and oxygen consumption rate. The phase differences between oxy- and deoxy-hemoglobin volume and flow phasors naturally emerge as the integrated effect of the RBCs moving from the arterioles, through capillaries and then to the venous compartment while exchanging oxygen with the surrounding tissue. As one application of the dynamic microcirculation PIPE model, we also present the solution of this model to quantitative coherent hemodynamics spectroscopy (CHS). Through analyzing both the cerebral and cutaneous coherent hemodynamics spectroscopy data, the performance of the PIPE model and the Fantini model [10] is compared, and the advantage of the PIPE model is demonstrated. The PIPE model is found to exhibit excellent agreement with the experimental data and identify more distinctively the impaired cerebral autoregulation in hemodialysis patients compared to healthy subjects than the Fantini model. The PIPE model is furthermore successfully used to interpret the fMRI-BOLD signal. This new dynamic microcirculation PIPE model provides a valuable tool for analyzing the signals measured by hemodynamic-based neuroimaging and non-neuroimaging techniques such as functional near-infrared spectroscopy (fNIRS) and functional magnetic resonance imaging (fMRI) in response to brain activation, physiological challenges, or physical maneuvers.

Biomedical Optics EXPRESS

2. The PIPE hemodynamics model

Both the hematocrit and the blood flow velocity vary inside the arterial, capillary, and venous compartments. We will make the following adjustments which simplify the model yet will alter neither the oxy-, deoxy- and total hemoglobin concentrations, the volume fractions of the arterial, capillary, and venous compartments throughout the vasculature, nor the transit times through the capillary and venous compartments, yielding identical measured optical or fMRI signals. First, the hemoglobin concentration in blood is assumed unchanged by regarding the blood volume as the effective volume incorporating the lower volume concentration of red blood cells within small blood vessels than that of blood entering or leaving the microvascular network because of the Fåhraeus effect [17]. We will further assume the average blood flow velocity is the same inside the capillaries and venules. The blood flow in capillaries is slower than that in the venule yet the total flow is conserved ($v_c A_c = v_v A_v$ with $v_{c,v}$ and $A_{c,v}$ representing the velocities and the total cross-section areas in the capillaries and venules, respectively). We will adjust the speed inside the venules to v_c and the total cross-section area to $A_v v_v/v_c$ while extending the length of the venules v_c/v_v times. This adjustment changes neither the total volume of the venules nor the transit time through the venules. These adjustments simplify the model notations below. The total cross-section area of the capillary and venous compartments is further assumed to be unity in the absence of the blood volume and flow variations.

Our formalism is developed after the above adjustments and with a convention of $\exp(-i\omega t)$ as the temporal dependence for a component of frequency ω. The physical quantities correspond to the real part of the complex values.

2.1. Nomenclature

The list of relevant hemodynamic quantities in the PIPE hemodynamics model:

$O(y,t)$: oxyhemoglobin content in blood per unit length (mmol/dm) along the pipe at position y and time t

$D(y,t)$: deoxy-hemoglobin content in blood per unit length along the pipe at position y and time t

$T(y,t)$: total hemoglobin content in blood per unit length along the pipe at position y and time t

$O(y,t)$, $D(y,t)$, $T(y,t)$ reduce to the oxy-, deoxy-, and total hemoglobin concentration (mmol/dm^3 = mM) in blood, respectively, in the absence of the blood volume and flow variations.

$\mathcal{O}(t)$: oxyhemoglobin concentration in tissue at time t

$\mathcal{D}(t)$: deoxy-hemoglobin concentration in tissue at time t

$\mathcal{T}(t)$: total hemoglobin concentration in tissue at time t

S_0: hemoglobin oxygen saturation inside the artery

t_c: mean blood transit time through the capillary compartment

t_v: mean blood transit time through the venous compartment

α: oxygen release rate to tissue

$\phi^{(a)}$, $\phi^{(c)}$, and $\phi^{(v)}$: the volume fraction of artery, capillary, and venule compartments in tissue, respectively, when the blood volume and flow variations are absent.

The tissue blood volume and flow velocity variation phasors for coherent hemodynamics spectroscopy are listed in Table 1.

Biomedical Optics EXPRESS

2.2. PIPE model

The arterioles, capillaries, and venules are treated as a complete network (*compliant* pipe) through which the total hemoglobin is conserved. The pipe may expand or constrict as the consequence of the blood volume and flow speed variations. We denote the blood oxyhemoglobin (HbO) content as $O(y,t)$ per unit length at position y and time t when the blood leaves the arterioles at $y = 0$, passes through capillaries of length L_c and merges into the vein through venule branches of length L_v. The quantity $O(y,t)$ reduces to the HbO concentration in blood when the blood volume and flow variations are absent and will vary due to blood volume variations caused by vascular dilation and constriction. Assuming the rate constant of oxygen release from hemoglobin to tissue (the oxygen diffusion constant from the capillary to tissue) is α, the local conservation law for HbO (see Fig. 1) leads to

$$\frac{\partial Q}{\partial y} + \frac{\partial O}{\partial t} = -\alpha O(y,t), \quad 0 \le y \le L_c \tag{1}$$

and

$$\frac{\partial Q}{\partial y} + \frac{\partial O}{\partial t} = 0, \quad L_c \le y \le L_c + L_v. \tag{2}$$

in the temporal domain where $Q(y,t) \equiv O(y,t)v(y,t)$ is the flow rate. A similar equation can be written for the total hemoglobin (THb) content in blood $T(y,t)$ with α set to be zero. The deoxy-hemoglobin content in the blood is $D \equiv T$ - O.

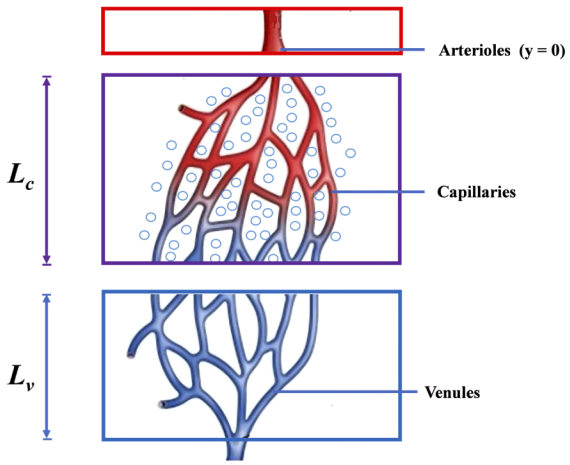

Fig. 1. The schematic diagram for the hemodynamics PIPE model.

We first consider the baseline case of the constant flow velocity $v = v_0$ and the constant oxygen diffusion rate α. The solution to (1) and (2) is given with the method of characteristics [18] by:

$$\begin{aligned} O_0(y,t) &= S_0 f(t - \frac{y}{v_0}) \exp(-\alpha \frac{y}{v_0}), \quad 0 \le y \le L_c \\ &= S_0 f(t - \frac{y}{v_0}) \exp(-\alpha t_c), \quad L_c \le y \le L_c + L_v, \end{aligned} \tag{3}$$

and

$$T(y,t) = f(t - \frac{y}{v_0}), \quad 0 \le y \le L_c + L_v \tag{4}$$

under a given boundary condition $T(0,t) = f(t)$ where $S_0 = 0.98$ is the value of the oxygen saturation in the artery, $f(t)$ specifies the total hemoglobin content in blood injected to the capillaries by the

Biomedical Optics EXPRESS

arterioles, $t_c \equiv L_c/v_0$ and $t_v = L_v/v_0$, are the mean blood transit times in the capillary and venous compartments, respectively. We have collapsed the artery within the probed volume into one single term at $y = 0$.

Now let's consider the perturbation on the blood flow velocity and the oxygen diffusion rate as $v(y, t) = v_0 + \delta v(y, t)$ and $\alpha + \delta\alpha(y, t)$, respectively. Equations (1) and (2) reduce to

$$\frac{\partial \delta O}{\partial y} v_0 + \frac{\partial \delta O}{\partial t} + \alpha \delta O = -\frac{\partial (O_0 \delta v)}{\partial y} - O_0 \delta\alpha, \quad 0 \le y \le L_c \tag{5}$$

and

$$\frac{\partial \delta O}{\partial y} v_0 + \frac{\partial \delta O}{\partial t} = -\frac{\partial (O_0 \delta v)}{\partial y}, \quad L_c \le y \le L_c + L_v \tag{6}$$

by retaining only up to the first order. The solution for δO to (5) and (6) is given by

$$\begin{aligned} \delta O(y,t) &= -v_0^{-1} \exp(-\frac{\alpha}{v_0} y) \int_0^y \exp(\frac{\alpha}{v_0}\xi) a(\xi, t - \frac{y-\xi}{v_0}) d\xi, \quad 0 \le y \le L_c \\ &= \delta O(L_c, t - \frac{y - L_c}{v_0}) - v_0^{-1} \int_{L_c}^y b(\xi, t - \frac{y-\xi}{v_0}) d\xi, \quad L_c \le y \le L_c + L_v \end{aligned} \tag{7}$$

where

$$a(y,t) \equiv \frac{\partial (O_0 \delta v)}{\partial y} + O_0 \delta\alpha \tag{8}$$

and

$$b(y,t) \equiv \frac{\partial (O_0 \delta v)}{\partial y} \tag{9}$$

imposing $\delta O(0, t) = 0$. The perturbation on THb, $\delta T(y, t)$, is obtained from (7) after setting $\alpha = 0$.

The detected optical or fMRI signal is determined by the average tissue oxy-, deoxy-, and total hemoglobin concentrations alone. Denote $\phi^{(a)}$, $\phi^{(c)}$, and $\phi^{(v)}$ as the volume fraction of artery, capillary, and venule compartments inside the tissue, respectively, when the blood volume and flow variations are absent. The baseline of tissue HbO concentration is given by

$$O_0(t) = S_0 \phi^{(a)} f(t) + S_0 \frac{\phi^{(c)}}{t_c} \int_0^{t_c} f(t-\tau) \exp(-\alpha\tau) d\tau + S_0 \frac{\phi^{(v)}}{t_v} \exp(-\alpha t_c) \int_{t_c}^{t_c + t_v} f(t-\tau) d\tau \tag{10}$$

The perturbation of tissue HbO concentration can be computed as the sum of contributions originating from δv and $\delta\alpha$, i.e.,

$$\delta O(t) = \delta O_{\delta v}(t) + \delta O_{\delta\alpha}(t) \tag{11}$$

where

$$\begin{aligned} \delta O_{\delta v}(t) = &-S_0 \frac{\phi^{(c)}}{v_0 t_c} \int_0^{t_c} d\tau [\exp(-\alpha t_c) f(t - t_c) \delta v(v_0 t_c - v_0 \tau, t - \tau) - \exp(-\alpha\tau) f(t-\tau) \delta v(0, t-\tau)] \\ &+ S_0 \frac{\phi^{(v)}}{v_0 t_v} \exp(-\alpha t_c) \left[\int_0^{t_c} d\tau f(t - t_c) \delta v(v_0 t_c - v_0 \tau, t - \tau) + \int_{t_c}^{t_c + t_v} d\tau f(t-\tau) \delta v(0, t-\tau) \right] \\ &- S_0 \frac{\phi^{(v)}}{v_0 t_v} \exp(-\alpha t_c) \left[\int_0^{t_v} \exp(-\alpha(t_v - \tau)) + \int_{t_v}^{t_c + t_v} \right] f(t - t_c - t_v) \delta v(v_0 t_c + v_0 t_v - v_0 \tau, t - \tau) d\tau \\ &+ S_0 \frac{\phi^{(v)}}{v_0 t_v} \alpha \exp(-\alpha t_c) \int_{t_c}^{t_c + t_v} d\tau f(t-\tau) \int_0^{t_c} \delta v(v_0 \tau', t - \tau + \tau') d\tau' \end{aligned} \tag{12}$$

Biomedical Optics EXPRESS

and

$$\begin{aligned}\delta O_{\delta\alpha}(t) = &-S_0\frac{\phi^{(c)}}{t_c}\int_0^{t_c} d\tau \exp(-\alpha\tau) f(t-\tau)\int_0^{\tau} d\tau' \delta\alpha(v_0\tau', t-\tau+\tau') \\ &- S_0\frac{\phi^{(v)}}{t_v}\exp(-\alpha t_c)\int_{t_c}^{t_c+t_v} d\tau f(t-\tau)\int_0^{t_c} d\tau' \delta\alpha(v_0\tau', t-\tau+\tau')\end{aligned} \tag{13}$$

Note the third line of (12) contains two integrals. The values of the baseline THb concentration $\mathcal{T}(t)$ and the perturbation $\delta\mathcal{T}(t)$ in tissue can be obtained from $O_0(t)$ and $\delta O(t)$ by setting $S_0 = 1$ and $\alpha = 0$. In particular,

$$\mathcal{T}(t) = \phi^{(a)} f(t) + \frac{\phi^{(c)}}{t_c}\int_0^{t_c} f(t-\tau)d\tau + \frac{\phi^{(v)}}{t_v}\int_{t_c}^{t_c+t_v} f(t-\tau)d\tau \tag{14}$$

and

$$\begin{aligned}\delta\mathcal{T}(t) = &-\frac{\phi^{(c)}}{v_0 t_c}\int_0^{t_c} d\tau[f(t-t_c)\delta v(v_0 t_c - v_0\tau, t-\tau) - f(t-\tau)\delta v(0, t-\tau)] \\ &+ \frac{\phi^{(v)}}{v_0 t_v}\left[\int_0^{t_c} d\tau f(t-t_c)\delta v(v_0 t_c - v_0\tau, t-\tau) + \int_{t_c}^{t_c+t_v} d\tau f(t-\tau)\delta v(0, t-\tau)\right] \\ &- \frac{\phi^{(v)}}{v_0 t_v}\int_0^{t_c+t_v} f(t-t_c-t_v)\delta v(v_0 t_c + v_0 t_v - v_0\tau, t-\tau)d\tau\end{aligned} \tag{15}$$

Equations (10–15) are the main equations describing the PIPE hemodynamics model, comprising of the baseline and volume variation contributions $O_0(t)$ and $\mathcal{T}(t)$, the flow velocity modulation contributions $\delta O_{\delta v}(t)$ and $\delta\mathcal{T}(t)$, and the oxygen release modulation contribution $\delta O_{\delta\alpha}(t)$ regarding the tissue oxy- and total hemoglobin concentrations. The PIPE hemodynamics model can admit arbitrary temporal modulation via the boundary condition $T(0,t) = f(t)$ specifying the total hemoglobin content in blood injected by the arterioles to the capillaries whose cross-section area is unity in the absence of blood volume and flow variations, which may represent brain activation, physiological challenges, or physical maneuvers. In the next subsection, a particular form of temporal modulation (sinusoidal) type is addressed, referred to as coherent hemodynamics.

2.3. Coherent hemodynamics spectroscopy (CHS)

In CHS, microcirculation is modulated by, for example, cuff pressure inflation/deflation or paced breathing at an angular frequency ω to introduce a periodic perturbation in the blood volume and flow speed. In this case, the coherent oscillation boundary condition at the arterioles $f(t)$ consists of both static and oscillatory components, $f(t) = T_0 + T_1\exp(-i\omega t)$, for the total hemoglobin content in blood injected to the capillaries by the arterioles. The baseline solution for the blood oxy- and total hemoglobin content in blood per unit length incorporating the contribution from volume oscillation is given by

$$\begin{aligned}O_0(y,t) &= S_0 T_0\exp(-\frac{\alpha}{v_0}y) + S_0 T_1\exp(-\frac{\alpha}{v_0}y)\exp\left(-i\omega t + i\frac{\omega}{v_0}y\right), \quad 0 \le y \le L_c \\ &= S_0 T_0\exp(-\alpha t_c) + S_0 T_1\exp(-\alpha t_c)\exp\left(-i\omega t + i\frac{\omega}{v_0}y\right), \quad L_c \le y \le L_c + L_v\end{aligned} \tag{16}$$

and

$$T(y,t) = T_0 + T_1\exp(-i\omega t + i\frac{\omega}{v_0}y), \quad 0 \le y \le L_c + L_v \tag{17}$$

The periodic blood volume variation is accompanied by the modulation in the flow velocity $v(0,t) = v_0 + v_1\exp(-i\omega t + i\theta)$ at this intersection position (the origin $y = 0$) where v_0 is the

Biomedical Optics EXPRESS

average blood velocity, v_1 is the amplitude of the velocity modulation, and $-\theta$ is the phase lead for the velocity modulation with respect to the volume oscillation at the arterioles. As a consequence, the flow velocity is no longer uniform inside the capillaries and venules, and the deviation from v_0 can be written as $\delta v(y,t) = v_1 \exp(iky - i\omega t + i\theta)$ where k is the wavevector given by $k = \omega/(v_0 + u)$ with u being the wave speed of the disturbance due to the velocity modulation. Inside the vessels of 0.1 mm or smaller (capillaries and venules), the flow is quasi-static and the ratio of $u/v_0 = \sqrt{\omega/2\pi f_{heart}} \ll 1$ where f_{heart} is the heartbeat frequency as the wave speed for small Womersley number pulsatile flow of angular frequency ω is proportional to $\sqrt{\omega}$ [19]. We further assume α is a constant (i.e., $\delta\alpha = 0$). Imposing $\delta O(0,\, t) = 0$, we find for $0 \le y \le L_c$

$$\begin{aligned}\delta O(y,t) = {} & S_0 T_0 \frac{v_1}{v_0}\left(\frac{\alpha}{v_0} - ik\right)\exp\left[-\frac{\alpha}{v_0}y - i\omega\left(t - \frac{y}{v_0}\right) + i\theta\right]\frac{\exp\left[\left(ik - \frac{i\omega}{v_0}\right)y\right] - 1}{ik - \frac{i\omega}{v_0}} \\ & + \frac{1}{2}S_0 T_1 \frac{v_1}{v_0}\left(\frac{\alpha - i\omega}{v_0} - ik\right)\exp\left[-\frac{\alpha}{v_0}y - i2\omega\left(t - \frac{y}{v_0}\right) + i\theta\right]\frac{\exp\left[\left(ik - \frac{i\omega}{v_0}\right)y\right] - 1}{ik - \frac{i\omega}{v_0}} \\ & - \frac{1}{2}S_0 T_1 \frac{v_1}{v_0}\left(ik + \frac{\alpha - i\omega}{v_0}\right)\exp\left(-\frac{\alpha}{v_0}y - i\theta\right)\frac{\exp\left[-\left(ik - \frac{i\omega}{v_0}\right)y\right] - 1}{ik - \frac{i\omega}{v_0}}.\end{aligned} \tag{18}$$

when $k \neq \omega/v_0$ and otherwise taken at the limit of $k = \omega/v_0$.

The solution for $L_c \le y \le L_c + L_v$ is given by

$$\begin{aligned}\delta O(y,t) = {} & \delta O\left(L_c, t - \frac{y - L_c}{v_0}\right) \\ & - S_0 T_0 \frac{v_1}{v_0}\frac{k}{k - \frac{\omega}{v_0}}\exp\left[-i\omega\left(t - \frac{y}{v_0}\right) + i\theta - \alpha t_c + \left(ik - \frac{i\omega}{v_0}\right)L_c\right]\left\{\exp\left[\left(ik - \frac{i\omega}{v_0}\right)(y - L_c)\right] - 1\right\} \\ & - \frac{1}{2}S_0 T_1 \frac{v_1}{v_0}\frac{k + \frac{\omega}{v_0}}{k - \frac{\omega}{v_0}}\exp\left[-i2\omega\left(t - \frac{y}{v_0}\right) + i\theta - \alpha t_c + \left(ik - \frac{i\omega}{v_0}\right)L_c\right]\left\{\exp\left[\left(ik - \frac{i\omega}{v_0}\right)(y - L_c)\right] - 1\right\} \\ & - \frac{1}{2}S_0 T_1 \frac{v_1}{v_0}\exp\left[-i\theta - \alpha t_c - \left(ik - \frac{i\omega}{v_0}\right)L_c\right]\left\{\exp\left[-\left(ik - \frac{i\omega}{v_0}\right)(y - L_c)\right] - 1\right\}.\end{aligned} \tag{19}$$

when $k \neq \omega/v_0$ and otherwise taken at the limit of $k = \omega/v_0$.

The velocity modulation produces the oscillations in O of DC, ω, and 2ω frequencies in time (see (18) and (19)). Typically, the 2ω oscillatory term is much weaker than the fundamental mode and can be ignored. The DC term, however, will alter the oxygen extraction rate. The time-averaged baseline oxygen extraction in unit time per unit volume of the capillary compartment:

$$E = \alpha S_0 T_0 \frac{1 - \exp(-\alpha t_c)}{\alpha t_c} \tag{20}$$

The value of E represents the number (moles) of HbO converted to Hb in unit time per unit volume of the capillary compartment. The DC term gives rise to the additional oxygen extraction in unit time per unit volume of the capillary compartment given by

$$\delta E = t_c^{-1}\frac{1}{2}S_0 T_1 \frac{v_1}{v_0}\exp(-i\theta)\left[1 - \exp(-\alpha t_c) + i\frac{\alpha}{kv_0 - \omega}(1 - \exp(-i(kv_0 - \omega)t_c))\exp(-\alpha t_c)\right] \tag{21}$$

when $k \neq \omega/v_0$ and otherwise taken at the limit of $k = \omega/v_0$. The ratio marks the oxygen extraction efficiency, and efficiency increases with shorter capillary transit time. By retaining only the

Biomedical Optics EXPRESS

leading exp(-$i\omega t$) oscillatory term in (18,19), the flow velocity modulation gives rise to

$$\begin{aligned}
&\delta O(y,t)\\
&= -S_0T_0\frac{v_1}{v_0}\frac{\beta+i\alpha}{\beta-\omega}\exp[-i\omega t+i\theta]\left\{\exp\left[-(\alpha-i\beta)\frac{y}{v_0}\right]-\exp\left[-(\alpha-i\omega)\frac{y}{v_0}\right]\right\}, \quad 0\le y\le L_c\\
&= -S_0T_0\frac{v_1}{v_0}\frac{\beta+i\alpha}{\beta-\omega}\exp\left[-i\omega t+i\theta-\alpha t_c+i\omega\frac{y}{v_0}\right]\{\exp[i(\beta-\omega)t_c]-1\}\\
&\quad -S_0T_0\frac{v_1}{v_0}\frac{\beta}{\beta-\omega}\exp[-i\omega t+i\theta-\alpha t_c+i\beta t_c]\left\{\exp\left[i\beta\frac{y}{v_0}-i\beta t_c\right]-\exp\left[i\omega\frac{y}{v_0}-i\omega t_c\right]\right\},\\
&\qquad\qquad L_c\le y\le L_c+L_v
\end{aligned} \tag{22}$$

where $\beta\equiv kv_0=\omega/(1+\sqrt{\omega/2\pi f_{heart}})$. A similar expression can be obtained for δT as (letting $S_0=1$ and $\alpha=0$):

$$\begin{aligned}
\delta T(y,t) &= -T_0\frac{v_1}{v_0}\frac{\beta}{\beta-\omega}\exp\left[-i\omega(t-\frac{y}{v_0})+i\theta\right]\left\{\exp\left[i(\beta-\omega)\frac{y}{v_0}\right]-1\right\}, \quad 0\le y\le L_c\\
&= -T_0\frac{v_1}{v_0}\frac{\beta}{\beta-\omega}\exp\left[-i\omega(t-\frac{y}{v_0})+i\theta\right]\{\exp[i(\beta-\omega)t_c]-1\}\\
&\quad -T_0\frac{v_1}{v_0}\frac{\beta}{\beta-\omega}\exp\left[-i\omega(t-\frac{y}{v_0})+i\theta\right]\left\{\exp\left[i(\beta-\omega)\frac{y}{v_0}\right]-\exp[i(\beta-\omega)t_c]\right\},\\
&\qquad\qquad L_c\le y\le L_c+L_v
\end{aligned} \tag{23}$$

Inside the interrogated volume, the baseline tissue oxyhemoglobin and total hemoglobin concentrations are then given by

$$\begin{aligned}
O_0(t) &= S_0T_0\left[\phi^{(a)}+\phi^{(c)}\frac{\exp(-\alpha t_c)-1}{-\alpha t_c}+\phi^{(v)}\exp(-\alpha t_c)\right]\\
&\quad +S_0T_1\exp(-i\omega t)\left[\phi^{(a)}+\phi^{(c)}\frac{\exp(-\alpha t_c+i\omega t_c)-1}{-\alpha t_c+i\omega t_c}+\phi^{(v)}\frac{\exp(i\omega t_v)-1}{i\omega t_v}\exp(-\alpha t_c+i\omega t_c)\right]
\end{aligned} \tag{24}$$

and

$$\begin{aligned}
\mathcal{T}(t) &= T_0(\phi^{(a)}+\phi^{(c)}+\phi^{(v)})\\
&\quad +T_1\exp(-i\omega t)\left[\phi^{(a)}+\phi^{(c)}\frac{\exp(i\omega t_c)-1}{i\omega t_c}+\phi^{(v)}\frac{\exp(i\omega t_v)-1}{i\omega t_v}\exp(i\omega t_c)\right],
\end{aligned} \tag{25}$$

respectively. The flow velocity modulation leads to perturbations in tissue oxyhemoglobin and total hemoglobin concentrations of

$$\begin{aligned}
\delta O(t) &= -\phi^{(c)}S_0T_0\frac{v_1}{v_0}\frac{\beta+i\alpha}{\beta-\omega}\exp[-i\omega t+i\theta]\left\{\frac{\exp[(i\beta-\alpha)t_c]-1}{(i\beta-\alpha)t_c}-\frac{\exp[(i\omega-\alpha)t_c]-1}{(i\omega-\alpha)t_c}\right\}\\
&\quad -\phi^{(v)}S_0T_0\frac{v_1}{v_0}\frac{\beta+i\alpha}{\beta-\omega}\exp[-i\omega t+i\theta-\alpha t_c]\frac{\exp(i\omega t_v)-1}{i\omega t_v}[\exp(i\beta t_c)-\exp(i\omega t_c)]\\
&\quad -\phi^{(v)}S_0T_0\frac{v_1}{v_0}\frac{\beta}{\beta-\omega}\exp[-i\omega t+i\theta-\alpha t_c+i\beta t_c]\left\{\frac{\exp(i\beta t_v)-1}{i\beta t_v}-\frac{\exp(i\omega t_v)-1}{i\omega t_v}\right\},
\end{aligned} \tag{26}$$

Biomedical Optics EXPRESS

and

$$\delta\mathcal{T}(t) = -\phi^{(c)}T_0\frac{v_1}{v_0}\frac{\beta}{\beta-\omega}\exp[-i\omega t + i\theta]\left\{\frac{\exp(i\beta t_c)-1}{i\beta t_c} - \frac{\exp(i\omega t_c)-1}{i\omega t_c}\right\}$$
$$-\phi^{(v)}T_0\frac{v_1}{v_0}\frac{\beta}{\beta-\omega}\exp[-i\omega t + i\theta]\left\{\exp(i\beta t_c)\frac{\exp(i\beta t_v)-1}{i\beta t_v} - \exp(i\omega t_c)\frac{\exp(i\omega t_v)-1}{i\omega t_v}\right\}. \quad (27)$$

Equations (24–27) are the main equations for CHS and will be the basis to analyze CHS measurements.

We could easily account for the distribution of the transit times t_c and t_v. One common used distribution [20] is a Gamma distribution, $\frac{1}{\Gamma(a)}\gamma^a x^{a-1}\exp(-\gamma x)$, of mean $\mu = a/\gamma$ and variance a/γ^2. This distribution has dispersion $\sigma^2 = (a/\gamma^2)/\mu^2 = 1/a$ and reduces to the exponential distribution when $a = 1$. The random variable t following such a Gamma distribution satisfies

$$\langle\exp(-\beta t)\rangle = \left(\frac{a}{a+\beta\mu}\right)^a \quad (28)$$

$$\langle\exp(-\beta t)\beta t\rangle = \beta\mu\left(\frac{a}{a+\beta\mu}\right)^{a+1} \quad (29)$$

and

$$\left\langle\frac{\exp(-\beta t)-1}{-\beta t}\right\rangle = \frac{a}{(-a+1)\beta\mu}\left[\left(\frac{a}{a+\beta\mu}\right)^{a-1} - 1\right]. \quad (30)$$

The formula for $O_0(t)$, $\delta O(t)$, $\mathcal{T}(t)$, and $\delta\mathcal{T}(t)$ in (24-27) are modified to account for the capillary and venule transit time distributions by substitution with the above rules when needed.

2.4. Specification of auto-regulation

The autoregulation is specified by how the flow velocity modulation relates to the pressure modulation. Un-impaired autoregulation is characterized by a smaller ratio between the amplitude of flow velocity modulation to the amplitude of the pressure modulation and a larger phase lead of the former than the latter [21]. The total hemoglobin volume oscillation is proportional and approximately in phase to that of the pressure, as observed by Reinhard et al. [22,23]. It is justified to model the autoregulation by relating the flow velocity modulation to the total hemoglobin volume modulation and write

$$\frac{\delta v(t)}{v_0} = k_g\int_0^\infty R(\tau)\frac{\delta T(t-\tau)}{T_0}d\tau \quad (31)$$

at the arterioles following [15] where δv represents the flow velocity modulation, and $k_g R(t)$ represents the autoregulation with k_g being the inverse of the modified Grubb's exponent. One common choice [15] for $R(t)$ is a resistor-capacitor high-pass impulse response function specified by

$$R(t) = -\frac{1}{\tau_c}\exp(-t/\tau_c) + \delta(t) \quad (32)$$

with time constant $\tau_c \equiv 1/\omega_c$, $\omega_c = 2\pi f_c$ being the cutoff angular frequency, and $\delta(t)$ being the Dirac delta function. In the frequency domain, the autoregulation can be written as

$$R(\omega) = \frac{1}{1 + i\omega_c/\omega} \quad (33)$$

in our convention of exp(-$i\omega t$) as the temporal dependence for a component of frequency ω. With the above model, the auto-regulation factor $v_1\exp(i\theta)/v_0$ in (26) and (27) of CHS is specified by $\upsilon R(\omega) = \upsilon/(1 + i\omega_c/\omega)$ where υ represents the flow velocity modulation ratio.

Biomedical Optics EXPRESS

2.5. Blood volume and flow velocity oscillation phasors

Hemodynamic variation is the superposition of blood volume and blood flow velocity oscillatory components when the rate of oxygen release to tissue can be regarded as constant. The oxy-, deoxy-, and total hemoglobin volume oscillation phasors, $\mathbf{O}_V$, $\mathbf{D}_V$, and $\mathbf{T}_V$, and the oxy-, deoxy-, and total hemoglobin flow velocity oscillation phasors, $\mathbf{O}_F$, $\mathbf{D}_F$, and $\mathbf{T}_F$ (see Table 1), respectively, can be recovered after fitting the CHS measurement to (24-27). The expressions for these phasors are summarized in Table 1.

Table 1. Expressions for Oxy-, Deoxy-, and Total Hemoglobin Volume and Velocity Oscillation Phasors. Here the Auto-regulation Factor $v_1 \exp(i\theta)/v_0$ is Specified by $\upsilon R(\omega) = \upsilon/(1 + i\omega_c/\omega)$ and β is Given by $\omega/(1 + \sqrt{\omega/2\pi f_{heart}})$. The Rules of (28-30) Should be Applied to Account for the Capillary and Venule Transit Time Distributions. The Temporal Dependence on the Angular Frequency ω Takes the Form of $\exp(-i\omega t)$.

Nomenclature	Expression
$\mathbf{O}_V$	$S_0 T_1 \left[\phi^{(a)} + \phi^{(c)} \frac{\exp(-\alpha t_c + i\omega t_c) - 1}{-\alpha t_c + i\omega t_c} + \phi^{(v)} \frac{\exp(i\omega t_v) - 1}{i\omega t_v} \exp(-\alpha t_c + i\omega t_c)\right]$
$\mathbf{T}_V$	$T_1 \left[\phi^{(a)} + \phi^{(c)} \frac{\exp(i\omega t_c) - 1}{i\omega t_c} + \phi^{(v)} \frac{\exp(i\omega t_v) - 1}{i\omega t_v} \exp(i\omega t_c)\right]$
$\mathbf{D}_V$	$\mathbf{T}_V$-$\mathbf{O}_V$
$\mathbf{O}_F$	$-\phi^{(c)} S_0 T_0 \frac{v_1}{v_0} \frac{\beta + i\alpha}{\beta - \omega} \exp(i\theta) \left\{\frac{\exp[(i\beta - \alpha)t_c] - 1}{(i\beta - \alpha)t_c} - \frac{\exp[(i\omega - \alpha)t_c] - 1}{(i\omega - \alpha)t_c}\right\}$ $-\phi^{(v)} S_0 T_0 \frac{v_1}{v_0} \frac{\beta + i\alpha}{\beta - \omega} \exp(i\theta - \alpha t_c) \frac{\exp(i\omega t_v) - 1}{i\omega t_v} [\exp(i\beta t_c) - \exp(i\omega t_c)]$ $-\phi^{(v)} S_0 T_0 \frac{v_1}{v_0} \frac{\beta}{\beta - \omega} \exp(i\theta - \alpha t_c + i\beta t_c) \left\{\frac{\exp(i\beta t_v) - 1}{i\beta t_v} - \frac{\exp(i\omega t_v) - 1}{i\omega t_v}\right\}.$
$\mathbf{T}_F$	$-\phi^{(c)} T_0 \frac{v_1}{v_0} \frac{\beta}{\beta - \omega} \exp(i\theta) \left\{\frac{\exp(i\beta t_c) - 1}{i\beta t_c} - \frac{\exp(i\omega t_c) - 1}{i\omega t_c}\right\}$ $-\phi^{(v)} T_0 \frac{v_1}{v_0} \frac{\beta}{\beta - \omega} \exp(i\theta) \left\{\exp(i\beta t_c) \frac{\exp(i\beta t_v) - 1}{i\beta t_v} - \exp(i\omega t_c) \frac{\exp(i\omega t_v) - 1}{i\omega t_v}\right\}$
$\mathbf{D}_F$	$\mathbf{T}_F$-$\mathbf{O}_F$
$\mathbf{O}$	$\mathbf{O}_F + \mathbf{O}_V$
$\mathbf{T}$	$\mathbf{T}_F + \mathbf{T}_V$
$\mathbf{D}$	$\mathbf{T}$– $\mathbf{O}$

2.6. Difference between the PIPE model and the Fantini model

Both Fantini and PIPE models regard the oscillatory hemodynamics introduced by, for example, periodic cuff pressure inflation/deflation or paced breathing as the sum of contributions due to blood volume and flow velocity oscillations from the arterial, capillary and venous compartments, respectively (when the oxygen diffusion rate is assumed to be a constant). The Fantini model assumes that the vascular components of the oxy- and deoxy-hemoglobin volume oscillation phasors ($\mathbf{O}_V^{(a)}$, $\mathbf{D}_V^{(a)}$, $\mathbf{O}_V^{(c)}$, $\mathbf{D}_V^{(c)}$, $\mathbf{O}_V^{(v)}$, and $\mathbf{D}_V^{(v)}$ where superscripts "(a)", "(c)", and "(v)" represent the arterioles, capillaries, and venules, respectively) are in phase within each compartment whereas the vascular components of the oxy- and deoxy-hemoglobin flow oscillation phasors ($\mathbf{O}_F^{(a)}$, $\mathbf{D}_F^{(a)}$, $\mathbf{O}_F^{(c)}$, $\mathbf{D}_F^{(c)}$, $\mathbf{O}_F^{(v)}$, and $\mathbf{D}_F^{(v)}$) are out of phase within each compartment. Neither the total oxy- and deoxy-hemoglobin volume oscillation phasors ($\mathbf{O}_V$, $\mathbf{D}_V$) as the sum of the three compartmental phasors are in phase nor the total oxy- and deoxy-hemoglobin flow velocity oscillation phasors ($\mathbf{O}_F$, $\mathbf{D}_F$) are out-of-phase in principle. The Fantini model, when applied to the analysis of experimental data, however, typically further made simplifications that the oxy- and deoxy-hemoglobin volume oscillations ($\mathbf{O}_V$, $\mathbf{D}_V$) are in phase whereas the oxy- and deoxy-hemoglobin flow velocity oscillations ($\mathbf{O}_F$, $\mathbf{D}_F$) are out-of-phase. By contrast, the PIPE model does not make any *a priori* assumptions on the phase relations between oxy- and deoxy-hemoglobin phasors. Based on the local conservation of the total hemoglobin and as the outcome of a rigorous fluid dynamics treatment, the oscillatory phase difference between volume and flow velocity oscillations naturally emerges in the PIPE model as the integrated effect of

Biomedical Optics EXPRESS

the RBCs moving from the arterioles, through capillaries and then to the venous compartment while exchanging oxygen with the surrounding tissue. The PIPE model furthermore can easily account for the heterogeneity in the capillary and venous transit times, using a simple procedure as described above. It will be demonstrated in the following section comparing the performance of both models on cerebral and cutaneous hemodynamics that the PIPE model exhibits excellent agreement with the experimental data and identifies more distinctively the impaired autoregulation of hemodialysis patients vs healthy subjects than the Fantini model.

We note that our formalism is developed with a convention of exp(-$i\omega t$) as the temporal dependence for a component of frequency ω and the physical quantities correspond to the real part of the complex values. The results reported in the Results and Discussion sections have been converted to the exp($i\omega t$) convention by taking the complex conjugate to conform to what being reported in Pierro et. al [14].

3. Experiment procedure and data analysis

3.1. Cerebral hemodynamics

The cerebral coherent hemodynamics data in Pierro et al. [14] was analyzed by the PIPE model and compared to the analysis with the Fantini model. An automated cuff inflation device (E-20 Rapid Cuff Inflation System, D. E. Hokanson, Inc., Bellevue, Washington) was used to induce cerebral hemodynamic oscillations at a set of frequencies in both healthy subjects (n = 6) and hemodialysis patients (n = 5) among whom 3 are glomerulonephritis patients and 2 are diabetes patients.

Specifically, the data for the 11 subjects were fitted using GlobalSearch with fmincon (Matlab, USA) to minimize the least-squares error defined by

$$\text{error} = \frac{1}{3n}\sum_{i=1}^{n}\left(\frac{|\text{OT}_i - ot_i|^2}{\overline{|ot|}^2} + \frac{|\text{DT}_i - dt_i|^2}{\overline{|dt|}^2} + \frac{|\text{DO}_i - do_i|^2}{\overline{|do|}^2}\right) \tag{34}$$

where OT, DT and DO are the theoretical complex values of the ratios **O/T**, **D/T** and **D/O** for phasors **O**, **D**, and **T** predicted by either the PIPE model (see Table 1) or the Fantini model, *ot*, *dt* and *do* is the measured complex **O/T**, **D/T,** and **D/O**, respectively, *n* is the total number of frequencies measured, and the subscript *i* represents the frequency index. The arithmetic average of the amplitude of *ot*, *dt*, and *do* is denoted by $\overline{|ot|}$, $\overline{|dt|}$, and $\overline{|do|}$, respectively.

The mean total hemoglobin concentration in the cerebral artery is assumed $T_0 = 2.3$ mM, the total hemoglobin oscillation $T_1 = 10\mu$M, and the oxygen diffusion constant $\alpha = 0.8\text{s}^{-1}$ following [14]. The typical capillary blood flow speed $v_c = v_0 = 1$ mm/s. The range of $\phi^{(a)}$, $\phi^{(c)}$, and $\phi^{(v)}$ can be determined from the blood volume fraction in brain tissue, and it was found to be ~1-1.5% for capillaries and ~2-4% for the entire vasculature [24]. The dispersion of the transit time is assumed to be between 0.03 and 0.55 for the venous transit time t_v [20]. No dispersion in the capillary transit time t_c is assumed. Fitting by the Fantini model follows [14]. The set of parameters fitted in the PIPE model include: capillary transit time t_c, venous transit time t_v and its dispersion σ, flow velocity modulation ratio ν, the cutoff angular frequency ω_c, and the volume fraction ratios $\phi^{(c)}/(\phi^{(a)} + \phi^{(c)} + \phi^{(v)})$ and $\phi^{(v)}/(\phi^{(a)} + \phi^{(c)} + \phi^{(v)})$.

The fitting of the PIPE model and the Fantini model is displayed in Fig. 2 and Fig. 3 for healthy subjects and hemodialysis patients. Both models fit the data well. In the Results and Discussion sections, the volume and flow velocity oscillations presented are at the frequency of 0.1 Hz.

3.2. Cutaneous hemodynamics

A Single Snapshot Multiple frequency Demodulation-Spatial Frequency Domain Imaging (SSMD-SFDI) system was used to image the opisthenar (back of the hand) of healthy volunteers

Biomedical Optics EXPRESS

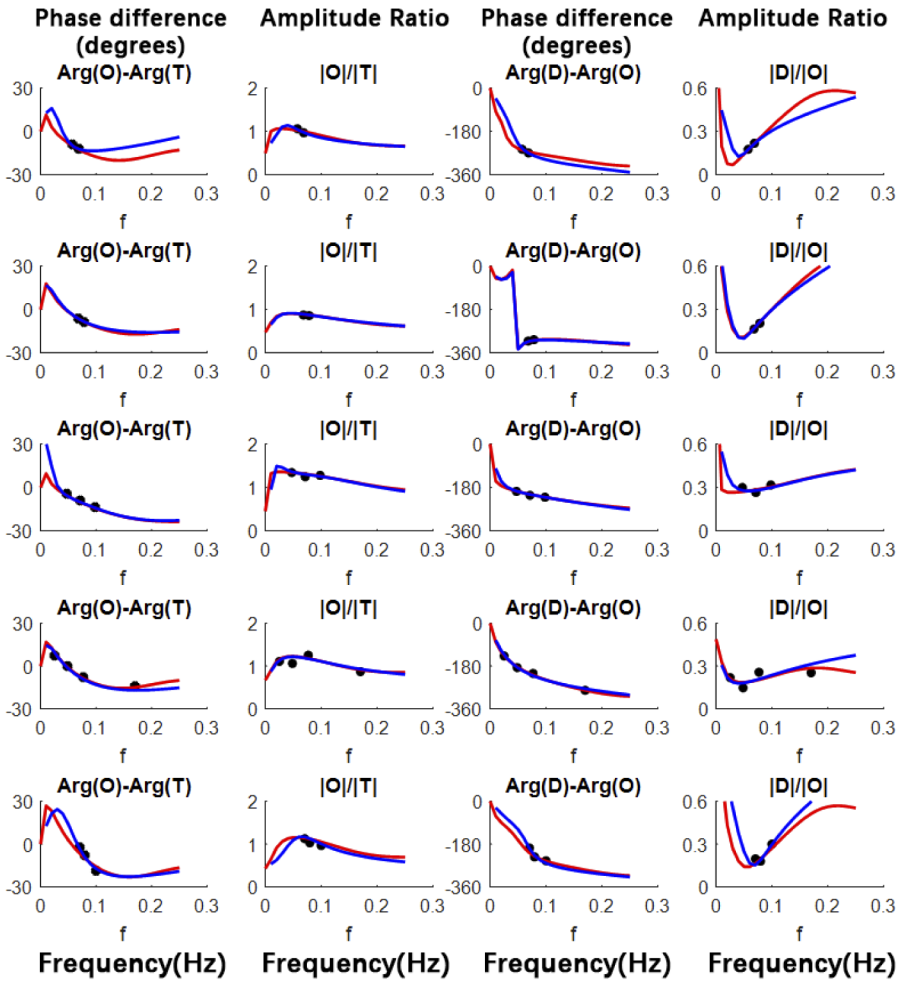

Fig. 2. Coherent hemodynamics spectra (CHS) measured on the forehead of five hemodialysis patients (Subjects 1 to 5 from top to bottom) fitted by the PIPE model (blue lines) and the Fantini model (red lines).

Biomedical Optics EXPRESS

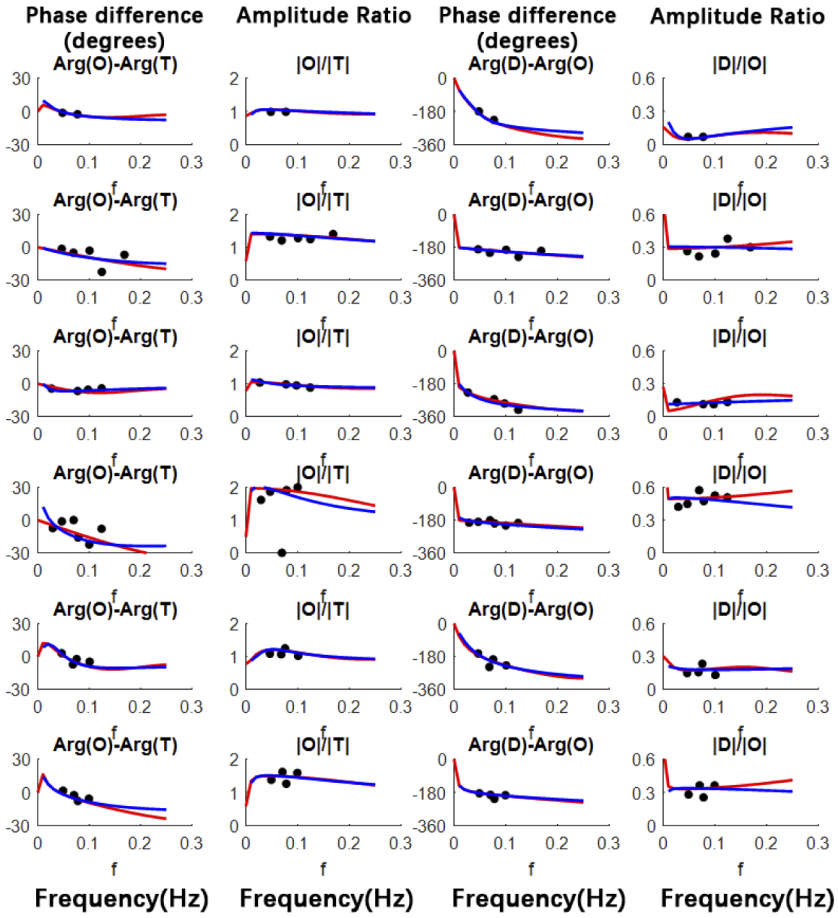

Fig. 3. Coherent hemodynamics spectra (CHS) measured on the forehead of six healthy subjects (Subjects 6 to 11 from top to bottom) fitted by the PIPE model (blue lines) and the Fantini model (red lines).

(n = 6) under the paced breathing protocol (f = 0.0625, 0.0714, 0.0833, 0.1000, 0.1250 Hz). The system has been described in [25]. Briefly, the sinusoidal fringe pattern on digital micromirror device (DMD, DLP LightCrafter 4500, Texas Instruments) is de-magnified and projected onto the opisthenar. Backscattered light was directly imaged onto the CCD camera (Point Gray Grasshopper3 GS3-U3-51S5C, USA). The illumination used white light which comprised three monochromatic components of the wavelengths of 623 nm, 540 nm, and 460 nm. During the experiments, the spatial modulation frequency of the white illumination light was 0.2 mm^{-1} on the surface of the specimen. The CCD exposure time was fixed at 20000 μs and the framerate was set at 5 fps. A region of interest (ROI) of size 5mm×5 mm within the image window was selected for data analysis. At each temporal point, Single Snapshot Multiple Frequency Demodulation (SSMD) [26] was used to compute the modulation transfer functions, $MTF_{DC} = I_{DC}/I_{DC}^{(0)}$ and $MTF_{AC} = I_{AC}/I_{AC}^{(0)}$, at the spatial frequencies f = 0 and 0.2 mm^{-1} for red, green, and blue light from the recorded color image over the ROI. The properties of the two-layer skin including oxy- and deoxy-hemoglobin concentrations, the reduced scattering coefficient at 540 nm, the scattering power, the melanin concentration, and the epidermal thickness were then fitted using

Biomedical Optics EXPRESS

the function fmincon in Matlab by minimizing the least squared error [25]:

$$\text{error} = \sum_{i=1}^{3} [(\text{MTF}_{\text{AC}}(\lambda_i) - \text{mtf}_{\text{AC}}(\lambda_i))^2 + (\text{MTF}_{\text{DC}}(\lambda_i) - \text{mtf}_{\text{DC}}(\lambda_i))^2] \tag{35}$$

where $i = 1,2,3$ represent the three colors, and the theoretical values of the modulation transfer functions, mtf_{DC} and mtf_{AC}, are computed with the enhanced diffusion model for the effective homogeneous medium [27–29].

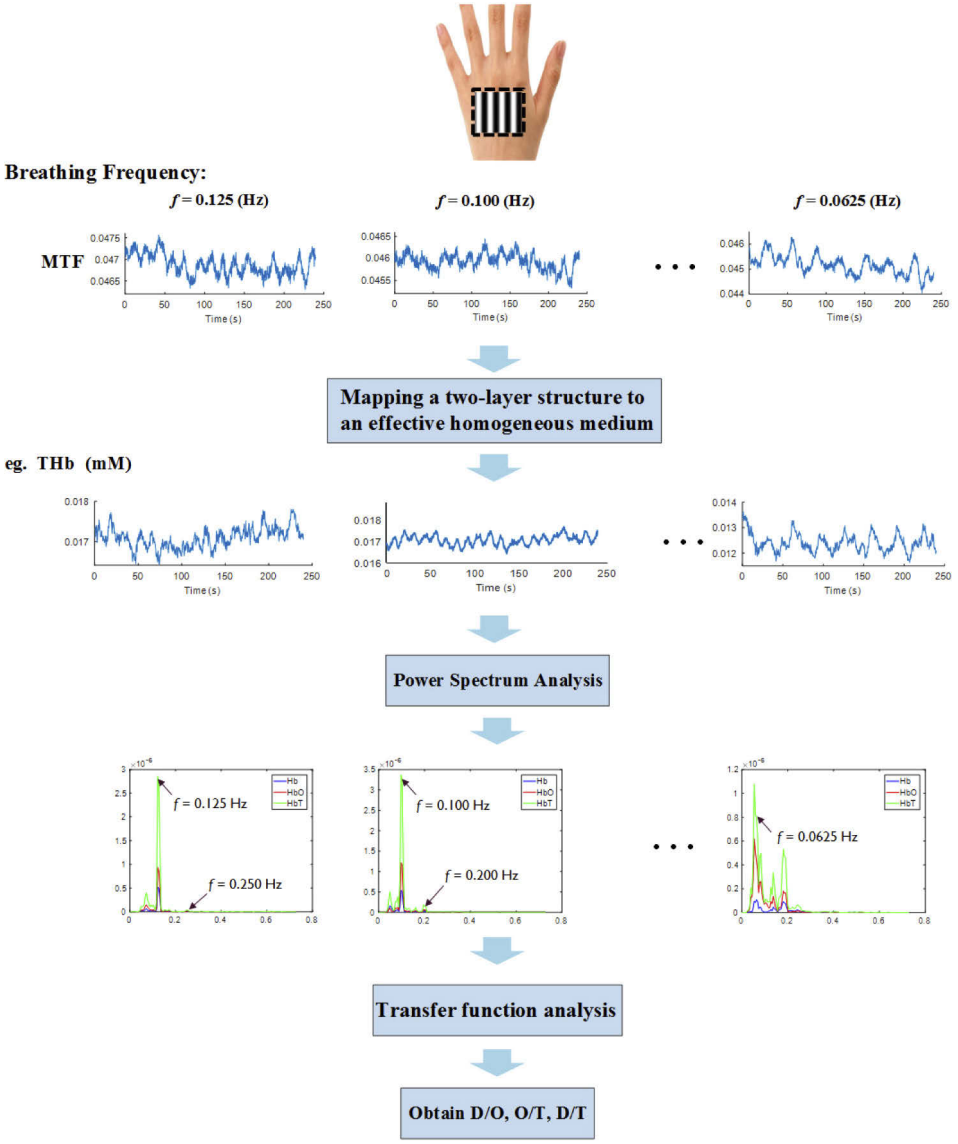

Fig. 4. Flow chart of the procedure for cutaneous coherent hemodynamics spectroscopy.

The recovered tissue deoxy-, oxy-, and total hemoglobin concentration temporal traces over 4 minutes were first median filtered and detrended by a third-order polynomial to obtain the time traces of oscillations $\mathcal{D}(t)$, $\mathcal{O}(t)$, and $\mathcal{T}(t)$. Power spectra analysis was used to confirm

Biomedical Optics EXPRESS

the presence of the induced oscillations (0.0625 to 0.125 Hz) and their bandwidth. A transfer function analysis was then conducted to extract coherent hemodynamic components within the identified bandwidth and determine the amplitude ratios ($|\mathbf{O}|/|\mathbf{T}|$, $|\mathbf{D}|/|\mathbf{T}|$, and $|\mathbf{D}|/|\mathbf{O}|$) and phase differences (Arg($\mathbf{D}$)-Arg($\mathbf{O}$), Arg($\mathbf{O}$)-Arg($\mathbf{T}$), and Arg($\mathbf{D}$)-Arg($\mathbf{T}$)). The oxygen diffusion coefficient in opisthenars is lower than that in brains and is set to $\alpha = 0.4\text{s}^{-1}$ [30]. The flow chart of the procedure is shown in Fig. 4. The identical fitting procedure as for the cerebral hemodynamics is then followed afterward. In the Results and Discussion sections, the volume and flow velocity oscillations presented are at the frequency of 0.1 Hz.

4. Results

4.1. Results of cerebral hemodynamics

Figure 5 summarizes the key hemodynamic characteristics for the five hemodialysis patients (subjects 1-5) and the six healthy subjects (subjects 6-11) fitted by the PIPE model (the blue lines and the blue diamond points) and the Fantini model (the red lines and the red square points). The blood transit time in the cerebral microcirculation is significantly longer in hemodialysis patients compared to healthy subjects in both models. The difference in the blood transit time in microcirculation is found to be t_c:1.14 ± 0.20 vs 0.41 ± 0.22 s, t_v: 4.72 ± 2.90 vs 1.75 ± 0.79 s in the PIPE model and t_c: 1.10 ± 0.23 vs 0.56 ± 0.18 s, t_v: 2.59 ± 0.83 vs 1.56 ± 0.74 s in the Fantini model, respectively. Furthermore, the autoregulation cutoff frequency ($\omega_c^{(autoReg)}/2\pi$) of the PIPE model ($0.056 \pm 0.030$ vs 0.011 ± 0.012 Hz) and the Fantini model (0.023 ± 0.017 vs 0.009 ± 0.007 Hz) are both larger for the hemodialysis patients than healthy subjects. The large dispersion in the venous transit time for the five hemodialysis patients recovered by the PIPE model is attributed to the fact that subjects 3 and 4 are diabetes, whereas the rest are glomerulonephritis patients (see Discussion and Table 5). The differences and the corresponding p-values from the t-test are given in Table 2.

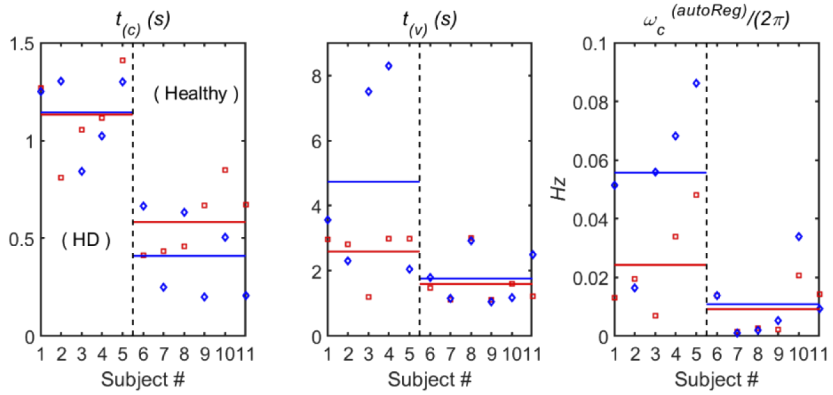

Fig. 5. Hemodynamic characteristics (t_c: capillary blood transit time, t_v: venous blood transit time, $\omega_c^{(autoReg)}/2\pi$: autoregulation cutoff frequency) for the five hemodialysis patients (subjects 1-5) and the six healthy subjects (subjects 6-11) fitted by the PIPE model (the blue lines and the blue diamond points) and the Fantini model (the red lines and the red square points). Horizontal lines represent the respective average values.

Hemodynamic variation is the superposition of blood volume and blood flow velocity oscillatory components when the rate of oxygen release to tissue is regarded as constant. Figure 6 displays the blood volume oscillation from the Fantini model (top row) and the PIPE model (bottom row). $\mathbf{O}_V$, $\mathbf{D}_V$, and $\mathbf{T}_V$ represent oxy-, deoxy-, and total hemoglobin volume oscillation phasors, respectively. Unlike the Fantini model, the PIPE model reveals that the phase lag of the deoxy-hemoglobin

Biomedical Optics EXPRESS

Table 2. Average Capillary Blood Transit Time, Venous Blood Transit Time, and Autoregulation Cutoff Frequency and Their *p*-Values from *t*-Tests Comparing Hemodialysis Patients and Healthy Subjects.

	Fantini model			PIPE model		
	Hemodialysis patients	Healthy subjects	*p*	Hemodialysis patients	Healthy subjects	*p*
t_c (s)	1.10 ± 0.23	0.56 ± 0.18	6E-4	1.14 ± 0.20	0.41 ± 0.22	3E-4
t_v (s)	2.59 ± 0.83	1.56 ± 0.74	0.06	4.72 ± 2.90	1.75 ± 0.79	0.06
$\omega_c^{(autoReg)}/2\pi(Hz)$	0.023 ± 0.017	0.009 ± 0.007	0.08	0.056 ± 0.030	0.011 ± 0.012	0.12

volume oscillation ($\mathbf{D}_V$) for hemodialysis patients is larger than that of healthy subjects as the result of the longer capillary transit time t_c for hemodialysis patients. Furthermore, the oxy- and deoxy-hemoglobin volume oscillation phasors $\mathbf{O}_V$ and $\mathbf{D}_V$ are not in phase from the PIPE model. The phase difference between $\mathbf{O}_V$ and $\mathbf{D}_V$ (Arg($\mathbf{O}_V$) – Arg($\mathbf{D}_V$)) is between 16° and 47° for hemodialysis patients and between 1.5° and 16° for healthy subjects in the PIPE model.

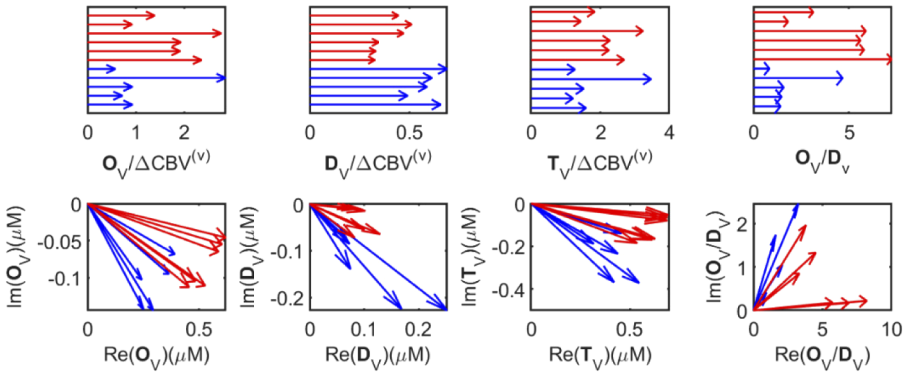

Fig. 6. The blood volume oscillation from the Fantini model (top row) and the PIPE model (bottom row). $\Delta CBV^{(v)}$ is the cerebral blood oscillation phasor defined in the Fantini model. $\mathbf{O}_v$, $\mathbf{D}_v$, and $\mathbf{T}_v$ represent oxy-, deoxy-, and total hemoglobin volume oscillation phasors, respectively. Red arrows represent healthy subjects and blue arrows represent hemodialysis patients.

Figure 7 displays the blood flow velocity oscillations from the Fantini model (top row) and the PIPE model (bottom row). $\mathbf{O}_F$, $\mathbf{D}_F$ and $\mathbf{T}_F$ represent oxy-, deoxy- and total hemoglobin flow velocity oscillations, respectively. $\mathbf{O}_F$ and $\mathbf{D}_F$ is absolutely out-of-phase and $\mathbf{T}_F = 0$ in the Fantini model. The PIPE model does not assume $\mathbf{O}_F$ and $\mathbf{D}_F$ to be out of phase. The phase difference between $\mathbf{O}_F$ and $\mathbf{D}_F$ (Arg ($\mathbf{O}_F$) – Arg ($\mathbf{D}_F$)) is between -79° and -123° for hemodialysis patients and between for -105° and -143° for healthy subjects in the PIPE model. The $\mathbf{T}_F$ amplitude of hemodialysis patients is found to be much greater than healthy subjects in the PIPE model, consistent with impaired autoregulation of the hemodialysis patients.

Cerebral autoregulation can be quantified by the relationship between the blood volume oscillation phasor, which can be regarded as a proxy for the arterial blood pressure oscillations, and the corresponding flow velocity oscillation phasor. The two ratios $\mathbf{O}_F/\mathbf{O}_V$ and $\mathbf{T}_F/\mathbf{T}_V$ are displayed in Fig. 8. The Fantini model does not reveal much difference in $\mathbf{O}_F/\mathbf{O}_V$ and $\mathbf{T}_F/\mathbf{T}_V$ (=0) between healthy subjects and hemodialysis patients. In contrast, the PIPE model shows that the amplitude ratios of $\mathbf{O}_F/\mathbf{O}_V$ and $\mathbf{T}_F/\mathbf{T}_V$ of hemodialysis patients are larger than that of healthy subjects, reflecting worse cerebral autoregulation of the former (see Table 3). The most distinctive characteristics of the impaired cerebral autoregulation of the hemodialysis patients

Biomedical Optics EXPRESS

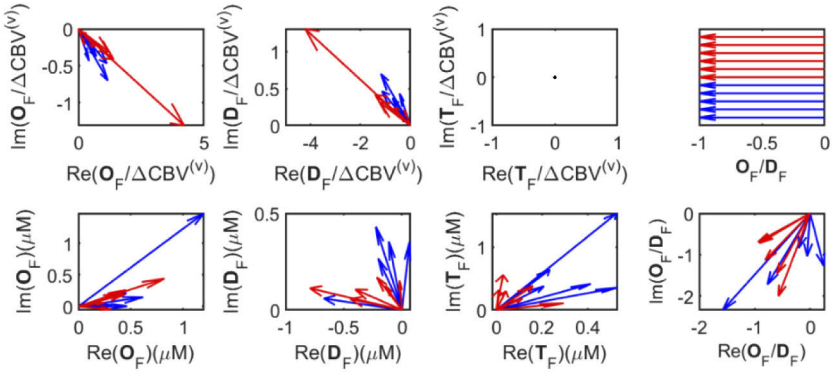

Fig. 7. The blood flow velocity oscillation for the Fantini model (top row) and the PIPE model (bottom row). $\mathbf{O}_F$, $\mathbf{D}_F$ and $\mathbf{T}_F$ represent oxy-, deoxy- and total hemoglobin flow oscillations, respectively. Red arrows represent healthy subjects and blue arrows represent hemodialysis patients.

show up in the larger amplitude ratio of the total hemoglobin flow velocity oscillation over the total hemoglobin volume oscillation ($|\mathbf{T}_F|/|\mathbf{T}_V|$).

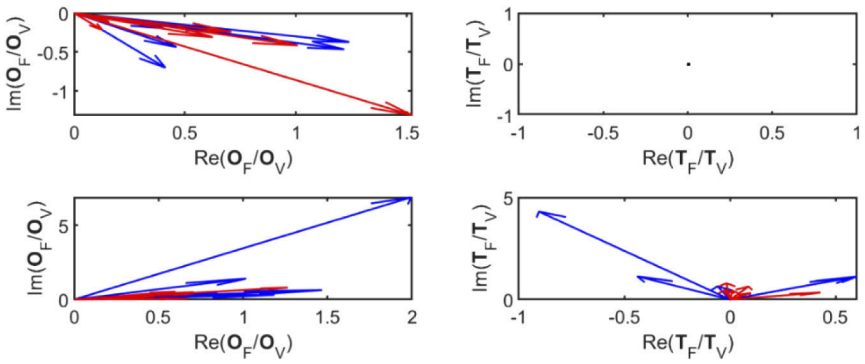

Fig. 8. Cerebral autoregulation $\mathbf{O}_F/\mathbf{O}_V$ and $\mathbf{T}_F/\mathbf{T}_V$ from the Fantini model (top row) and the PIPE model (bottom row). The ratio $\mathbf{T}_F/\mathbf{T}_V$ reduces to zero in the Fantini model (the top right panel). Red arrows represent healthy subjects and blue arrows represent hemodialysis patients.

Table 3. Cerebral Autoregulation of Hemodialysis Patients vs Healthy Subjects.

	Fantini model			PIPE model		
	Hemodialysis patients	Healthy subjects	p	Hemodialysis patients	Healthy subjects	p
$\lvert\mathbf{O}_F\rvert/\lvert\mathbf{O}_V\rvert$	0.87 ± 0.45	0.73 ± 0.55	0.67	2.55 ± 2.61	0.86 ± 0.34	0.15
$\lvert\mathbf{T}_F\rvert/\lvert\mathbf{T}_V\rvert$	-	-	-	1.75 ± 1.50	0.53 ± 0.16	0.07

4.2. Results of cutaneous hemodynamics

Figure 9 displays cutaneous hemodynamic characteristics for six healthy subjects fitted by the PIPE model (the blue lines and the blue diamond points) and the Fantini model (the red lines and the red square points). The blood transit time in the cutaneous microcirculation is longer than that

Biomedical Optics EXPRESS

in cerebral hemodynamics in both models. The autoregulation cutoff frequency $\omega_c^{(autoReg)}/2\pi$ is smaller from the PIPE model than that from the Fantini model. The observed cutaneous capillary transit time t_c is slightly larger in the PIPE model than that from the Fantini model. The longer cutaneous capillary transit time than the cerebral capillary transit time is consistent with the much lower oxygen diffusion rate in opisthenars than in brains and the higher oxygen extraction efficiency in the brain than the opisthenar (see (20), (21), and Discussion). The range of the cutaneous transit times is similar to the reported capillary transit time in muscles [31,32].

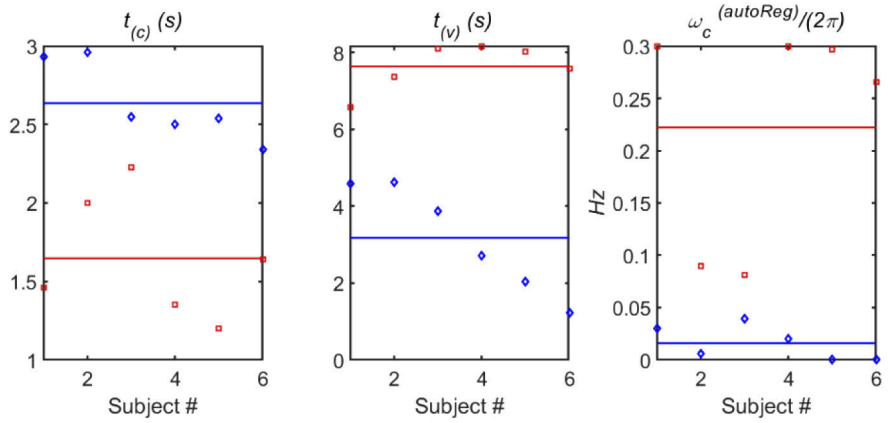

Fig. 9. Cutaneous hemodynamic characteristics (t_c: capillary blood transit time, t_v: venous blood transit time, $\omega_c^{(autoReg)}/2\pi$: autoregulation cutoff frequency) for four healthy subjects fitted by the PIPE model (the blue lines and the blue diamond points) and the Fantini model (the red lines and the red square points). Horizontal lines represent the respective average values.

Figure 10 displays the cutaneous blood volume oscillation from the Fantini model (top row) and the PIPE model (bottom row). The PIPE model reveals that the phase lag of the cutaneous deoxy-hemoglobin volume oscillation ($\mathbf{D}_V$) is larger than that in the brain for healthy subjects due to the longer capillary transit time t_c in the opisthenar. The total hemoglobin volume oscillation ($\mathbf{T}_V$) amplitudes of healthy subjects are similar in brains and opisthenars. The phase difference between $\mathbf{O}_V$ and $\mathbf{D}_V$ (Arg ($\mathbf{O}_V$) – Arg ($\mathbf{D}_V$)) is between 24° and 47° for healthy subjects in the PIPE model.

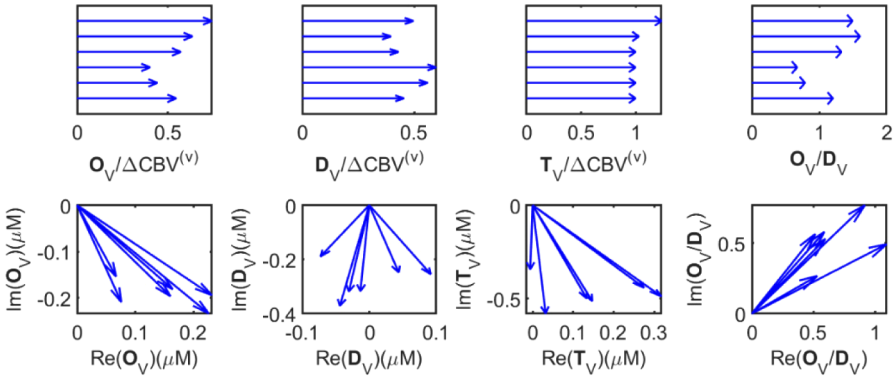

Fig. 10. The cutaneous blood volume oscillation from the Fantini model (top row) and the PIPE model (bottom row). $\mathbf{O}_V$, $\mathbf{D}_V$, and $\mathbf{T}_V$ represent oxy-, deoxy-, and total hemoglobin volume oscillations, respectively.

Biomedical Optics EXPRESS

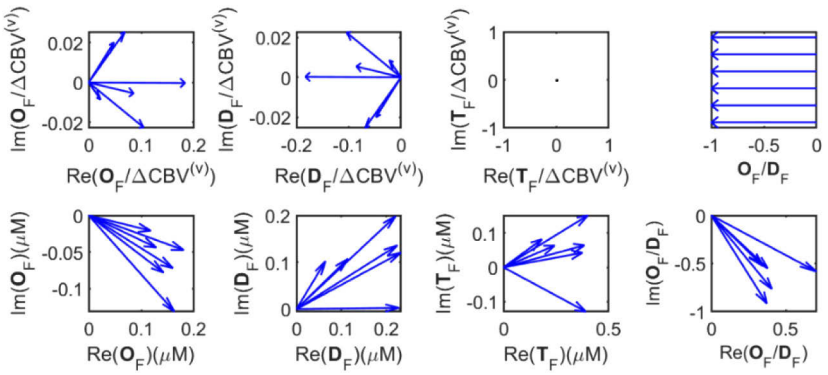

Fig. 11. The cutaneous blood flow velocity oscillation for the Fantini model (top row) and the PIPE model (bottom row). $\mathbf{O}_F$, $\mathbf{D}_F$ and $\mathbf{T}_F$ represent oxy-, deoxy- and total hemoglobin flow oscillations, respectively.

Figure 11 displays the cutaneous blood flow velocity oscillations from the Fantini model (top row) and the PIPE model (bottom row). $\mathbf{O}_F$ and $\mathbf{D}_F$ is absolutely out-of-phase and $\mathbf{T}_F = 0$ in the Fantini model. The phase difference between $\mathbf{O}_F$ and $\mathbf{D}_F$ (Arg ($\mathbf{O}_F$) – Arg ($\mathbf{D}_F$)) is between -39° and -67° for healthy subjects in the PIPE model. The $\mathbf{T}_F$ amplitude is similar in opisthenars and brains for healthy subjects. Figure 12 compares the cutaneous autoregulation $\mathbf{O}_F/\mathbf{O}_V$ and $\mathbf{T}_F/\mathbf{T}_V$ from the Fantini model (top row) and the PIPE model (bottom row). Table 4 summarizes $|\mathbf{O}_F|/|\mathbf{O}_V|$ and $|\mathbf{T}_F|/|\mathbf{T}_V|$ in brains and opisthenars for healthy subjects. Both ratios are similar in brains and opisthenars for healthy subjects in the PIPE model.

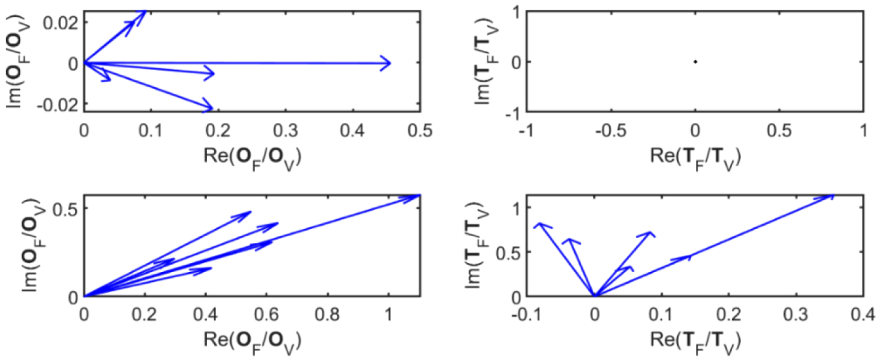

Fig. 12. Cutaneous autoregulation $\mathbf{O}_F/\mathbf{O}_V$ and $\mathbf{T}_F/\mathbf{T}_V$ from the Fantini model (top row) and the PIPE model (bottom row). $\mathbf{O}_F/\mathbf{O}_V$ and $\mathbf{T}_F/\mathbf{T}_V$ reflect the subject's opisthenar autoregulation.

Table 4. $|\mathbf{O}_F|/|\mathbf{O}_V|$ and $|\mathbf{T}_F|/|\mathbf{T}_V|$ in Brain and Opisthenar for Healthy Subjects

		$\lvert\mathbf{O}_F\rvert/\lvert\mathbf{O}_V\rvert$	$\lvert\mathbf{T}_F\rvert/\lvert\mathbf{T}_V\rvert$
Fantini Model	Brain	0.73 ± 0.55	-
	Opisthenar	0.18 ± 0.15	-
PIPE Model	Brain	0.86 ± 0.34	0.53 ± 0.16
	Opisthenar	0.70 ± 0.30	0.71 ± 0.30

Biomedical Optics EXPRESS

4.3. Application to fMRI

In addition to the application to functional optical spectroscopy of hemodynamics, the PIPE model can interpret the BOLD signal in functional magnetic resonance imaging (fMRI). The BOLD signal reflects a change in local deoxy-hemoglobin related to both blood flow and venous blood volume and metabolic response in oxygen metabolism. Adopting the same expression (47) in [10] for the BOLD signal, its temporal profile can be computed using (10-15).

Figure 13 shows one example of the application of the PIPE model to the BOLD signal. Similar to Pierro et al. [11], we extracted the fMRI BOLD data from Kida et al. [33] for two stimulus durations (4 s and 16 s) for the transient relative blood flow velocity change ($\delta v/v_0$) and the transient relative blood volume change ($(f-T_0)/T_0$). We then complemented it with the relative changes in the metabolic rate ($\Delta\alpha/\alpha$) according to Hyder et al. [34]. The BOLD signal was then calculated based on the deoxy-hemoglobin temporal trace from (10-15), assuming typical cerebral hemodynamic parameters as made in Pierro et al. [11]. The BOLD signal calculated with the PIPE model (short dash lines), the Fantini model (long dash lines) as well as the BOLD signal measured by Kida et al. [33] (solid lines) is shown in Fig. 13 for comparison. The calculated BOLD traces by both PIPE and Fantini models closely match the measured ones in terms of both shape and magnitude, except that the Fantini model predicts a slightly delayed onset in the BOLD signal.

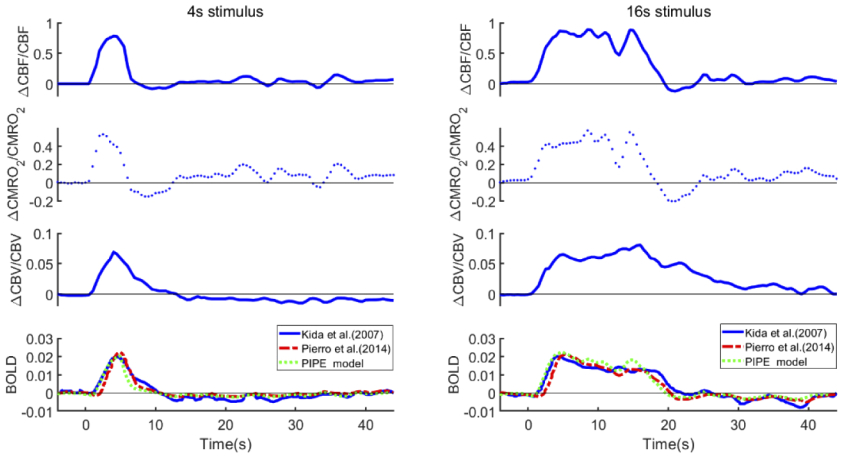

Fig. 13. BOLD fMRI study on rats. Left: 4s forepaw stimulation; Right: 16s forepaw stimulation. The top three panels are the relative changes in cerebral blood flow (ΔCBF/CBF), the metabolic rate of oxygen (ΔCMRO2/CMRO2), and cerebral blood volume (ΔCBV/CBV) derived from the data reported by Kida et al. [33] as described in the text. The bottom panel shows the BOLD fMRI signal measured by Kida et al. [33] using fMRI (solid line), and those predicted by the PIPE model (short dash lines) and the Fantini model (long dash lines).

5. Discussion

The central common feature of both Fantini and PIPE models for dynamic microcirculation is to interpret the hemodynamics as the superposition of the contributions from the blood volume variations, flow velocity modulations, and the rate of oxygen release variations within a network comprised of the arterial, capillary and venous compartments. The Fantini model assumes that the vascular components of the oxy- and deoxy-hemoglobin volume oscillation phasors ($\mathbf{O}_V^{(a)}$, $\mathbf{D}_V^{(a)}$, $\mathbf{O}_V^{(c)}$, $\mathbf{D}_V^{(c)}$, $\mathbf{O}_V^{(v)}$, and $\mathbf{D}_V^{(v)}$) are in phase within each compartment whereas the vascular components of the oxy- and deoxy-hemoglobin flow oscillation phasors ($\mathbf{O}_F^{(a)}$, $\mathbf{D}_F^{(a)}$,

Biomedical Optics EXPRESS

$\mathbf{O}_F^{(c)}$, $\mathbf{D}_F^{(c)}$, $\mathbf{O}_F^{(v)}$, and $\mathbf{D}_F^{(v)}$) are out of phase within each compartment. Neither the total oxy- and deoxy-hemoglobin volume oscillation phasors ($\mathbf{O}_V$, $\mathbf{D}_V$) are in phase nor the total oxy- and deoxy-hemoglobin flow velocity oscillation phasors ($\mathbf{O}_F$, $\mathbf{D}_F$) are out-of-phase, in principle, in the Fantini model. Simplifications were, however, typically introduced when applied to the analysis of experimental data that the oxy- and deoxy-hemoglobin volume oscillation phasors ($\mathbf{O}_V$, $\mathbf{D}_V$) are in phase and the oxy- and deoxy-hemoglobin flow velocity oscillation phasors ($\mathbf{O}_F$, $\mathbf{D}_F$) are out-of-phase in the Fantini model. By contrast, in the PIPE model the oscillatory phase difference between volume and flow velocity oscillations naturally emerges as the integrated effect of the RBCs moving from the arterioles, through capillaries and then to the venous compartment while exchanging oxygen with the surrounding tissue based on the conservation of the total hemoglobin alone. The phase difference between $\mathbf{O}_V$ and $\mathbf{D}_V$ (Arg($\mathbf{O}_V$) – Arg($\mathbf{D}_V$)) is between 16° and 47° for hemodialysis patients and between 1.5° and 16° for healthy subjects whereas the phase difference between $\mathbf{O}_F$ and $\mathbf{D}_F$ (Arg($\mathbf{O}_F$) – Arg($\mathbf{D}_F$)) is between -79° and -123° for hemodialysis patients and between for -105° and -143° for healthy subjects in brains as found by the PIPE model. Furthermore, the PIPE model predicts a weaker second harmonic mode in addition to the fundamental mode in CHS (see (18) and (19)). This behavior has been indeed observed in the cutaneous experimental data (see the insets in Fig. 4). The PIPE model can also easily account for the heterogeneity in the capillary and venous transit times.

The PIPE model is not only found to capture the microcirculation characteristics well but also reveals the distinctive hemodynamic parameters between hemodialysis patients and healthy subjects better than the Fantini model. For example, the impaired autoregulation of hemodialysis patients vs healthy subjects is much more revealed by the PIPE model (see Fig. 8 and Table 3).

The mean capillary oxygen saturation (ScO_2) can be evaluated by $S_0[1-\exp(-\alpha t_c)]/\alpha t_c$. Both the Fantini model and the PIPE model produce similar ScO_2 and find ScO_2 is lower for hemodialysis patients compared to healthy subjects (see Fig. 14). Furthermore, the cutaneous capillary oxygen saturation is found to be lower than the cerebral capillary oxygen saturation for healthy subjects. The lower ScO_2 from the PIPE model than the Fantini model for opisthenars is owing to the longer capillary transit time found in the former.

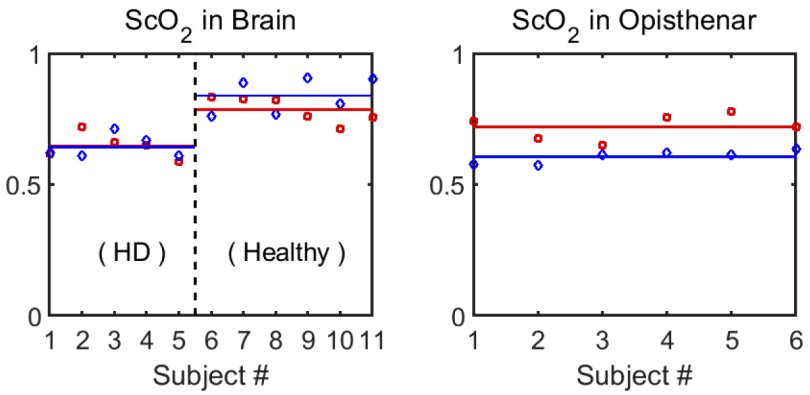

Fig. 14. Mean capillary oxygen saturation in (a) brain and (b)opisthenar by the PIPE model (the blue lines and the blue diamond points) and the Fantini model (the red lines and the red square points).

The baseline oxygen extraction efficiency E/T_0 is plotted in Fig. 15. The value of E/T_0 in the brain is lower for hemodialysis patients than that for healthy subjects. The value of E/T_0 in the brain is also much higher than that in opisthenar for healthy subjects. Figure 16 displays the oxygen extraction efficiency enhancement ($\delta E/T_0$) owing to the cyclic thigh cuff inflation/deflation

Biomedical Optics EXPRESS

or paced breathing. The oxygen extraction efficiency enhancement is found to be positive in all cases.

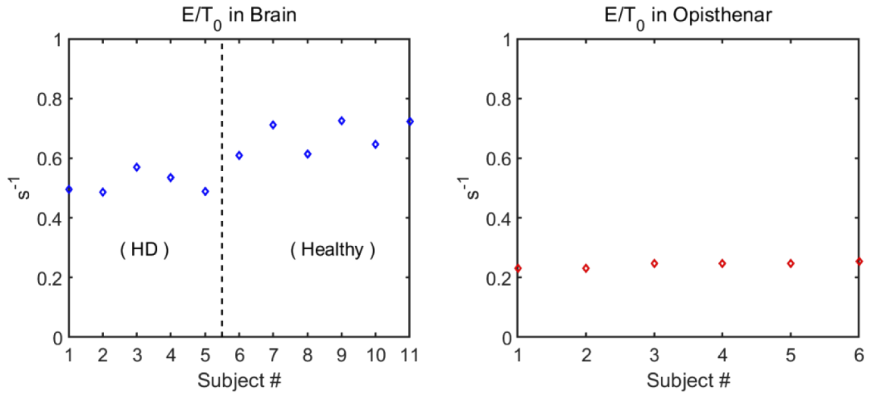

Fig. 15. The baseline oxygen extraction efficiency E/T_0 in (a) brain (the blue diamond points) and (b) opisthenar (the red square points) from the PIPE model.

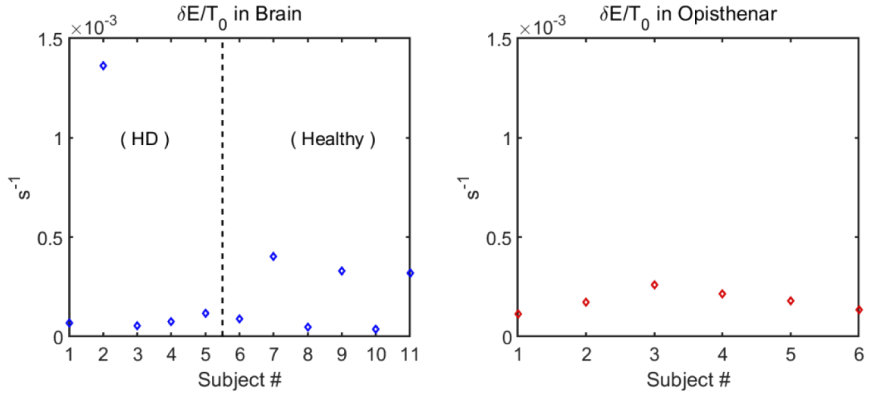

Fig. 16. The oxygen extraction efficiency enhancement $\delta E/T_0$ in (a) brain (the blue diamond points) and (b) opisthenar (the red square points) from the PIPE model.

We note that the five hemodialysis patients include three glomerulonephritis patients and two diabetes patients. The recovered hemodynamic parameters t_c, t_v, and ScO_2 of these patients are shown in Table 5. It is worth pointing out hemodialysis patients of diabetes have much greater t_v and larger ScO_2 than the hemodialysis patients with glomerulonephritis from the PIPE model, whereas no clear difference between these two groups of patients was observed from the Fantini model. The much longer venous transit time for diabetes patients reflects the impaired vasodilatation and vascular alterations due to diabetes mellitus [35]. Idle capillaries in the microvasculature, however, are recruited to compensate for this dysfunction, leading to the capillary transit time to not increase as much with diabetes.

Finally, we want to note that NIRS requires *a priori* knowledge of the scattering property of the medium for the recovery of the hemodynamics information. The spatial frequency domain imaging (SFDI) [25,36,37] used in our cutaneous hemodynamics study is a non-contact near-infrared (NIR) imaging approach that enables rapid, quantitative determination of both absorption and scattering properties. It hence removes the potential compounding issue of an

Biomedical Optics EXPRESS

Table 5. t_c, t_v, ScO_2 of Hemodialysis Patients

	The PIPE Model			The Fantini Model		
	t_c (s)	t_v(s)	ScO_2 (%)	t_c (s)	t_v (s)	ScO_2 (%)
Glomerulonephritis	1.25	3.56	61.9	1.27	2.97	61.5
	1.04	2.30	60.8	0.81	2.81	72.1
	1.30	1.79	60.9	1.41	2.99	58.7
Diabetes	0.84	7.49	71.3	1.05	1.20	66.2
	1.02	8.29	66.9	1.12	2.99	64.8

unknown or inaccurate scattering parameter comparing to NIRS. SFDI can furthermore provide *in vivo* rapid wide field-of-view imaging of hemodynamics, which will be of importance in the investigation of temporal and spatial dynamics of microcirculation.

6. Conclusion

In conclusion, we have presented a dynamic microcirculation PIPE model for functional neuroimaging, non-neuroimaging, and coherent hemodynamics spectroscopy. The temporal evolution of the concentration and oxygen saturation of hemoglobin in tissue is determined by time-resolved hemodynamic and metabolic variations in blood volume, flow velocity, and oxygen consumption in microvasculature comprised of the arterioles, capillaries, and venules as a complete network (*compliant* pipe) through which the total hemoglobin is conserved. Without making assumptions on the details of the architecture and morphology of the microvascular bed, the temporal connection and the phase relation between oxy- and deoxy-hemoglobin volume and flow velocity variations naturally emerges from the rigorous fluid dynamic treatment of the oxygen consumption occurring over the whole trajectory along which the red blood cells (RBC) move from the arterioles, through capillaries and then to the venous compartment while exchanging oxygen with the surrounding tissue. The dynamic microcirculation PIPE model provides a framework to assess key microcirculation parameters, including the effective blood transit time through the capillaries, the rate constant of oxygen release from hemoglobin to tissue, and the effective blood transit time through the venules. The vascular autoregulation can further be quantified from the relationship between the resolved blood volume and flow velocity variations.

We have also presented the solution of this dynamic microcirculation PIPE model to quantitative coherent hemodynamics spectroscopy. The PIPE model not only described the oscillatory hemodynamics in both brains and opisthenars satisfactorily but also identified more distinctively the impaired cerebral autoregulation in hemodialysis patients compared to healthy subjects than the Fantini model. The dynamic microcirculation PIPE model will be instrumental in recovering rich physiological information from analyzing and interpreting the signals measured by hemodynamic-based neuroimaging and non-neuroimaging techniques such as fNIRS and fMRI in response to brain activation, physiological challenges, or physical maneuvers.

Funding

Key Research Program of Zhejiang Natural Science Foundation of China (LZ16H180002); Wenzhou Municipal Science and Technology Bureau (ZS2017022); National Science Foundation (1607664); Welfare Project of Zhejiang Natural Science Foundation of China (LGF18H180013); National Natural Science Foundation of China (81470081).

Disclosures

The authors declare no conflicts of interest.

Biomedical Optics EXPRESS

References

1. M. Reinhard, T. Muller, B. Guschlbauer, J. Timmer, and A. Hetzel, "Transfer function analysis for clinical evaluation of dynamic cerebral autoregulation-a comparison between spontaneous and respiratory-induced oscillations," Physiol. Meas. **24**(1), 27–43 (2003).
2. L. Hughson R, R. Edwards M, D. O'Leary D, and K. Shoemaker J, "Critical analysis of cerebrovascular autoregulation during repeated head-up tilt," Stroke **32**(10), 2403–2408 (2001).
3. C. Jurgen A H R, L. Benjamin D, and Z. Rong, "Dynamic cerebral autoregulation during repeated squat-stand maneuvers," J. Appl. Physiol. **106**(1), 153–160 (2009).
4. A. Rune, B. Martin, S. Gill, M. Douville Colleen, and W. Newell David, "Asymmetric dynamic cerebral autoregulatory response to cyclic stimuli," Stroke **38**(5), 1465–1469 (2007).
5. F. Michael D and R. Marcus E, "Spontaneous fluctuations in brain activity observed with functional magnetic resonance imaging," Nat. Rev. Neurosci. **8**(9), 700–711 (2007).
6. B. R. White, A. Z. Snyder, A. L. Cohen, S. E. Petersen, M. E. Raichle, B. L. Schlaggar, and J. P. Culver, "Resting-state functional connectivity in the human brain revealed with diffuse optical tomography," NeuroImage **47**(1), 148–156 (2009).
7. A. Sassaroli, F. Zheng, M. Pierro, P. R. Bergethon, and S. Fantini, "Phase difference between low-frequency oscillations of cerebral deoxy- and oxyhemoglobin concentrations during a mental task," J. Innov. Opt. Health Sci. **04**(02), 151–158 (2011).
8. M. L. Pierro, A. Sassaroli, P. R. Bergethon, B. L. Ehrenberg, and S. Fantini, "Phase-amplitude investigation of spontaneous low-frequency oscillations of cerebral hemodynamics with near-infrared spectroscopy: A sleep study in human subjects," NeuroImage **63**(3), 1571–1584 (2012).
9. R. R. Diehl, D. Linden, D. Lücke, and P. Berlit, "Spontaneous blood pressure oscillations and cerebral autoregulation," Clin. Auton. Res. **8**(1), 7–12 (1998).
10. S. Fantini, "Dynamic model for the tissue concentration and oxygen saturation of hemoglobin in relation to blood volume, flow velocity, and oxygen consumption: Implications for functional neuroimaging and coherent hemodynamics spectroscopy (CHS)," NeuroImage **85**, 202–221 (2014).
11. M. L. Pierro, B. Hallacoglu, A. Sassaroli, J. M. Kainerstorfer, and S. Fantini, "Validation of a novel hemodynamic model for coherent hemodynamics spectroscopy (CHS) and functional brain studies with fNIRS and fMRI," NeuroImage **85**, 222–233 (2014).
12. R. B. Buxton, E. C. Wong, and L. R. Frank, "Dynamics of blood flow and oxygenation changes during brain activation: The balloon model," Magn. Reson. Med. **39**(6), 855–864 (1998).
13. B. Mandeville, J. J. A. Marota, M. A. Moskowitz, R. Rosen, and M. Weisskoff, "Evidence of a cerebrovascular postarteriole Windkessel with delayed compliance," J. Cereb. Blood Flow Metab. **19**(6), 679–689 (1999).
14. M. L. Pierro, J. M. Kainerstorfer, A. Civiletto, D. E. Weiner, A. Sassaroli, B. Hallacoglu, and S. Fantini, "Reduced speed of microvascular blood flow in hemodialysis patients versus healthy controls: a coherent hemodynamics spectroscopy study," J. Biomed. Opt. **19**(2), 026005 (2014).
15. J. M. Kainerstorfer, A. Sassaroli, K. T. Tgavalekos, and S. Fantini, "Dynamic cerebral autoregulation measured with coherent hemodynamics spectroscopy (CHS)," Proc. SPIE **9319**, 931901 (2015).
16. T. Pham, A. Sassaroli, G. Blaney, and S. Fantini, "Dynamic measurements of absolute cerebral blood flow with coherent hemodynamics spectroscopy," Proc. SPIE **10874**, 49 (2019).
17. R. Fahraeus and T. Lindqvist, "The viscosity of the blood in narrow capillary tubes," Am. J. Physiol. **96**(3), 562–568 (1931).
18. F. John, *Partial Differential Equations* (Springer, Berlin, 1991).
19. F. N. van de Vosse and N. Stergiopulos, "Pulse wave propagation in the arterial tree," Annu. Rev. Fluid Mech. **43**(1), 467–499 (2011).
20. R. B. King, G. M. Raymond, and J. B. Bassingthwaighte, "Modeling blood flow heterogeneity," Ann. Biomed. Eng. **24**(3), 352–372 (1996).
21. A. H. E. A. Van Beek, J. A. H. R. Claassen, M. G. M. O. Rikkert, and R. W. M. M. Jansen, "Cerebral autoregulation: An overview of current concepts and methodology with special focus on the elderly," J. Cereb. Blood Flow Metab. **28**(6), 1071–1085 (2008).
22. M. Reinhard, E. Wehrle-Wieland, D. Grabiak, M. Roth, B. Guschlbauer, J. Timmer, C. Weiller, and A. Hetzel, "Oscillatory cerebral hemodynamics—the macro- vs. microvascular level," J. Neurol. Sci. **250**(1-2), 103–109 (2006).
23. M. Ursino and A. Lodi C, "A simple mathematical model of the interaction between intracranial pressure and cerebral hemodynamics," J. Appl. Physiol. **82**(4), 1256–1269 (1997).
24. C. Francis, L. Frederic, F. Céline, P. Steffen, and L. C. Valerie, "A novel three-dimensional computer-assisted method for a quantitative study of microvascular networks of the human cerebral cortex," Microcirculation **13**(1), 1–18 (2016).
25. X. Chen, W. Lin, C. Wang, S. Chen, J. Sheng, B. Zeng, and M. Xu, "*In vivo* real-time imaging of cutaneous hemoglobin concentration, oxygen saturation, scattering properties, melanin content, and epidermal thickness with visible spatially modulated light," Biomed. Opt. Express **8**(12), 5468 (2017).
26. M. Xu, Z. Cao, W. Lin, X. Chen, L. Zheng, and B. Zeng, "Single snapshot multiple frequency modulated imaging of subsurface optical properties of turbid media with structured light," AIP Adv. **6**(12), 125208 (2016).

Biomedical Optics EXPRESS

27. M. Reilly and M. Xu, "Analytical model for sub-diffusive light reflection and the application to spatial frequency-domain imaging," Proc. SPIE **9319**, 93191A (2015).
28. M. Xu, "Low-coherence enhanced backscattering beyond diffusion," Opt. Lett. **33**(11), 1246–1248 (2008).
29. M. Xu, "Diagnosis of the phase function of random media from light reflectance," Sci. Rep. **6**(1), 22535 (2016).
30. K. Akons, E. J. Dann, and D. Yelin, "Measuring blood oxygen saturation along a capillary vessel in human," Biomed. Opt. Express **8**(11), 5342–5348 (2017).
31. C. R. Honig, M. L. Feldstein, and J. L. Frierson, "Capillary lengths, anastomoses, and estimated capillary transit times in skeletal muscle," Am. J. Physiol. - Hear. Circ. Physiol. **233**(1), H122–H129 (1977).
32. B. Klitzman and P. C. Johnson, "Capillary network geometry and red cell distribution in hamster cremaster muscle," Am. J. Physiol. - Hear. Circ. Physiol. **242**(2), H211–H219 (1982).
33. I. Kida, D. L. Rothman, and F. Hyder, "Dynamics of changes in blood flow, volume, and oxygenation: Implications for dynamic functional magnetic resonance imaging calibration," J. Cereb. Blood Flow Metab. **27**(4), 690–696 (2007).
34. F. Hyder, I. Kida, K. L. Behar, R. P. Kennan, P. K. Maciejewski, and D. L. Rothman, "Quantitative functional imaging of the brain: Towards mapping neuronal activity by BOLD fMRI," NMR Biomed. **14**(7-8), 413–431 (2001).
35. A. S. De Vriese, T. J. Verbeuren, J. de Voorde, N. H. Lameire, and P. M. Vanhoutte, "Endothelial dysfunction in diabetes," Br. J. Pharmacol. **130**(5), 963–974 (2000).
36. W. Lin, B. Zeng, Z. Cao, X. Chen, and M. Xu, "Quantitative diagnosis of tissue microstructure with wide-field high spatial frequency domain imaging," Biomed. Opt. Express **9**(7), 2905–2916 (2018).
37. M. Xu, "Plum pudding random medium model of biological tissue toward remote microscopy from spectroscopic light scattering," Biomed. Opt. Express **8**(6), 2879–2895 (2017).